minerals

MDPI

Article

Evolution of Syenite Magmas: Insights from the Geology, Geochemistry and O-Nd Isotopic Characteristics of the Ordovician Saibar Intrusion, Altai-Sayan Area, Russia

Alexander A. Vorontsov [1,2,*], Andrey E. Izoh [3], Vladimir V. Yarmolyuk [4], Tatyana Y. Komaritsyna [1], Anatoly V. Nikiforov [4], Olga Y. Perfilova [5], Sergei I. Dril [1], Nailya G. Rizvanova [6] and Egor P. Dushkin [1,2]

1 Institute of Geochemistry, Siberian Branch of the Russian Academy of Sciences, Favorskiy st. 1-a, 664033 Irkutsk, Russia; tkomaricina@mail.ru (T.Y.K.); sdril@igc.irk.ru (S.I.D.); egor.dushkin.99@mail.ru (E.P.D.)
2 Faculty of Geology, Irkutsk State University, 664033 Irkutsk, Russia
3 Institute of Geology and Mineralogy, Siberian Branch of the Russian Academy of Sciences, Academician Koptyug, av.3, 630090 Novosibirsk, Russia; izokh@igm.nsc.ru
4 Institute of Geology of Ore Deposits, Petrography, Mineralogy and Geochemistry, Russian Academy of Sciences, Staromonetny per. 35, 119017 Moscow, Russia; yarm1945@mail.ru (V.V.Y.); nikav@igem.ru (A.V.N.)
5 Department of Mining, Geology and Geotechnology, Siberian Federal University, Svobodniy, av. 79, 660041 Krasnoyarsk, Russia; perfil57@mail.ru
6 Institute of Precambrian Geology and Geochronology of the Russian Academy of Sciences, Makarova, nab. 2, 199034 St. Petersburg, Russia; rizng@mail.ru
* Correspondence: voront@igc.irk.ru; Tel.: +7-(92)-4510-0559

Abstract: In this paper, we provide insight into the evolution of syenite magmas based on geological data and petrographic, geochemical, and O-Nd isotope parameters of rocks of the Saibar intrusion located within the Minusinsk Trough, Altay-Sayan area. The intrusive suite includes predominant syenites, few bodies of melanocratic and leucocratic nepheline syenites (foyaites), and granites. In addition, dykes of granites and mafic rocks are present. The U-Pb zircon age from the melanocratic foyaites was determined to be 457 ± 10 Ma? Examined rocks show fractionated light rare earth element patterns, normalized to chondrite, with $(La/Sm)_n$ varying from 4 to 9, and a weakly fractionated distribution of medium and heavy rare elements, with $(Dy/Yb)_n$ from 0.35 to 1.23 and $(Sm/Yb)_n$ from 0.63 to 2.62. The spidergram normalized to the primitive mantle shows negative Ba, Sr, Nb, Ta, Ti, and Eu anomalies (Eu* = 0.48–0.60) and positive Rb, Th, and U anomalies. The $\delta^{18}O$ values vary within 6.3 to 10.2‰, and εNd(t) from +4.1 to +5.0. We observe gradual transitions from syenites to foyaites. Assimilation by syenite magma of the host carbonate rocks was followed to transition from silica-saturated to silica-undersaturated conditions and removal of anorthite from the melt, which then led to nepheline. Granites of the main phase show depleted lithophile incompatible elements in comparison with syenites and foyaites. They originate via interaction of magmas at the marginal part (endocontact zone) of the intrusion, corresponding to north contact of the granites with the host felsic rocks. In comparison, the rock composition of granite dykes is enriched in lithophile incompatible elements, except for Zr, Hf, and Ti. These rocks are formed due to the differentiation of syenite magma without a significant effect of host rock assimilation. Mantle magmas must be used as parent magmas for syenites based on analysis of the formation model of other alkaline intrusions, which are similar in age to the Saibar intrusion. In the line of syenite intrusions of the Altai-Sayan province, the Saibar intrusion is no exception, and its origin is related to the evolution of mafic magmas that arose during the melting of the mantle under the influence of a mantle plume.

Keywords: Saibar intrusion; Altai-Sayan area; Russia; Ordovician magmatism; alkaline magmas; fractionation; contamination; Minusinsk Trough

Citation: Vorontsov, A.A.; Izoh, A.E.; Yarmolyuk, V.V.; Komaritsyna, T.Y.; Nikiforov, A.V.; Perfilova, O.Y.; Dril, S.I.; Rizvanova, N.G.; Dushkin, E.P. Evolution of Syenite Magmas: Insights from the Geology, Geochemistry and O-Nd Isotopic Characteristics of the Ordovician Saibar Intrusion, Altai-Sayan Area, Russia. *Minerals* **2021**, *11*, 473. https://doi.org/10.3390/min11050473

Academic Editor: Silvio Giuseppe Rotolo

Received: 18 February 2021
Accepted: 27 April 2021
Published: 30 April 2021

1. Introduction

The main characteristics of syenites are sodium alkaline pyroxenes and amphiboles [1]. Syenites are relatively rare rocks related to alkaline and moderately alkaline magmatic associations of the continental region. These rocks are distributed together with ultramafic foidolites (ijolites, melteigites, urtite, and feldspathoid ijolites), alkaline gabbro, nepheline syenites (foyaites), carbonatites, and granites. The formation of syenites is associated with the characteristics of the evolution of mantle (model group 1), crustal (model group 2), and mantle-crustal (model group 3) sources of magmatic melts. Petrogenesis constraints are based on the analysis of geological, geochronological, and isotope-geochemical information. In the first group of models, the development of syenites is linked with mantle plume activity [2–5] coupled with continental rifting and differentiation of alkaline magmas of mafic composition [6–9]. Group 2 envisages melting of crustal substrates [10–12]. Group 3 considers mixing of mafic and felsic magmas, formation of hybrid melts and their subsequent differentiation [13–15], and mixing of silica undersaturated alkaline magmas of mantle origin with crustal granitic magmas [16]. We thoroughly investigated the evolution of syenite magmas in the western part of the Central Asian Orogenic Belt (CAOB, Figure 1a), including its history from the Neoproterozoic to the Late Paleozoic [17–31]. This part of the CAOB covers the sizable Altay-Sayan fold belt, where alkaline magmatism produced the syenites typical of Kuznetsk Alatau and southeast of Tuva in the Eastern Sayan Mountains and Sangilen Highland, as well as in the Minusinsk Trough subdividing these territories. Alkaline magmatism proceeded several times throughout the Paleozoic epoch in the Early Paleozoic (510–450 Ma), Devonian (410–390 Ma), and Late Carboniferous and Early Permian (305–280 Ma) [32–46].

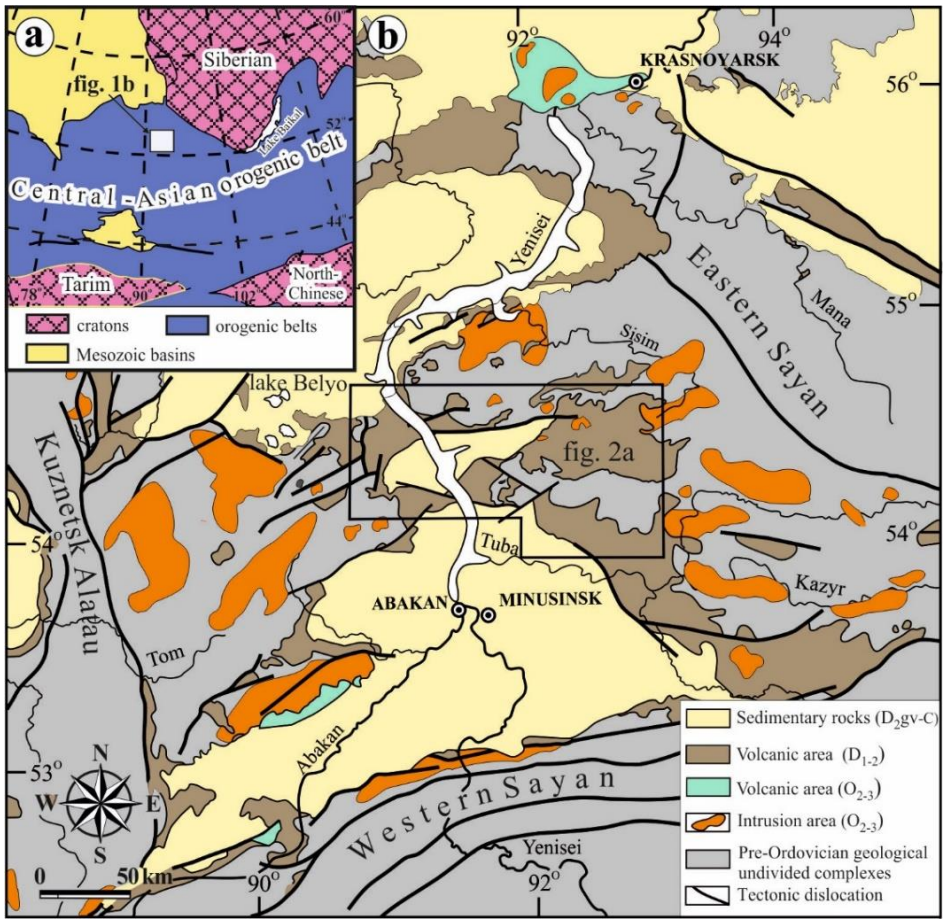

Figure 1. (**a**) Location of the Minusinsk Trough in the Central Asian orogenic belt. (**b**) Early Middle Paleozoic magmatic areas of the Minusinsk Trough; data source from [47,48].

This paper presents the results of our study of Ordovician syenites, foyaites, and granites of the Saibar intrusion, which is typical of a large group of Early Paleozoic syenite intrusions within the Minusinsk Trough (Figure 1b), located in the eastern part of Altai-Sayan region. A comprehensive study of this intrusion contributes to understanding the petrological and geodynamic mechanisms responsible for alkaline magmatism in the Altai-Sayan region.

2. Geological Background and Petrography

Intrusions, primarily composed of quartz syenites, syenites, and granites, occur in the mountainous surroundings of the Syda-Erba depression (Figure 2a), enclosed in the Minusinsk Trough [49]. They enclose the "Saibar group" consisting of the Saibar (Figure 2b), Burovskiy, Kosmatiy, and Vysokiy intrusions, which contain both alkali quartz and nepheline syenites.

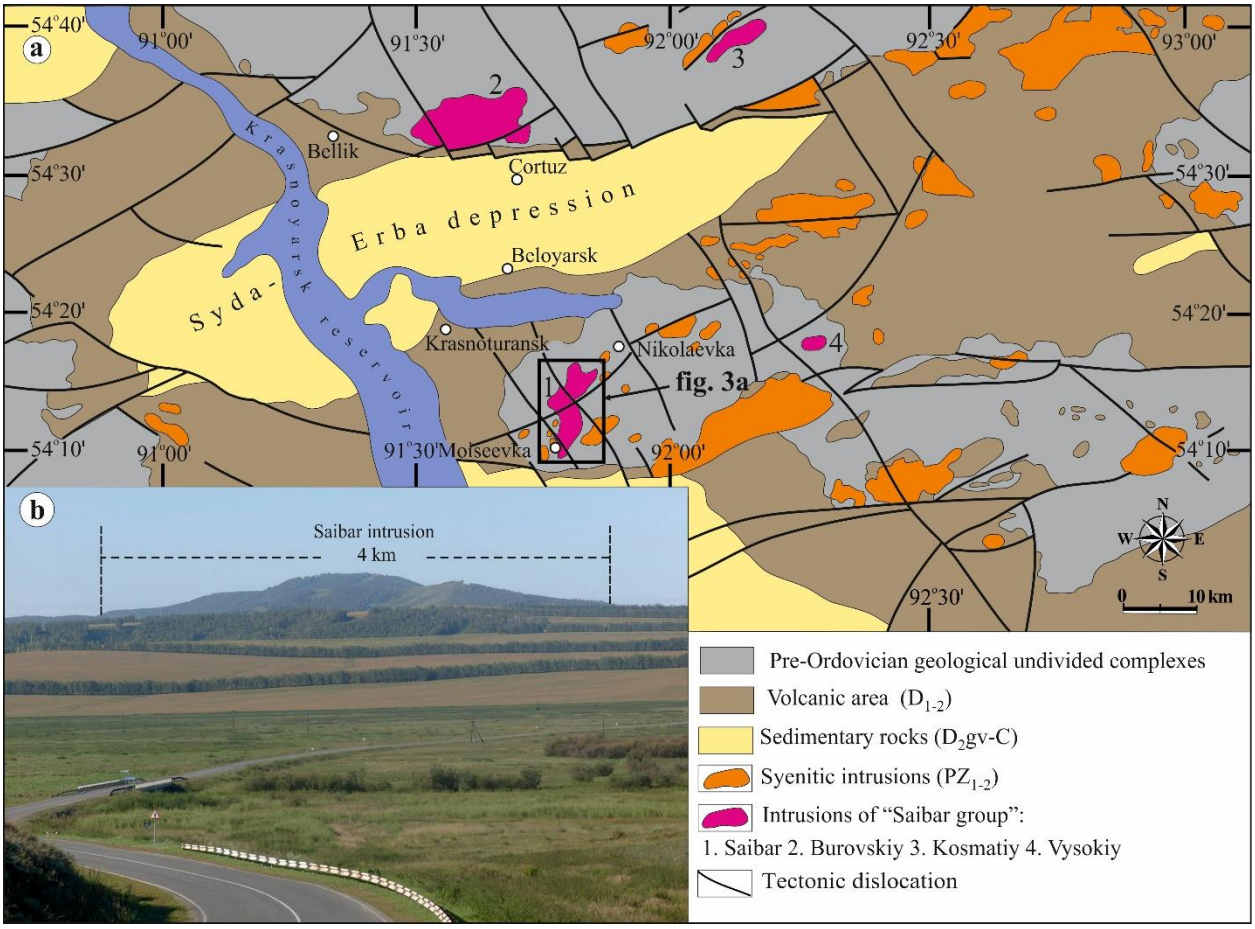

Figure 2. (**a**) Location of syenite-granite intrusions in the Syda-Erba depression of the Minusinsk Trough, modified from [49]. (**b**) Representative photos showing survey panorama of the Saibar intrusion; the distance to the peak of the intrusion is about 10 km (view from the side of the Nikolaevka village).

Pre-Ordovician felsic magmatic associations and Cambrian sedimentary deposits (siliceous shales, limestones, sandstones) are host rocks for this group of intrusions. In this group, the Saibar intrusion (Figure 3a) is considered a representative, since it contains the most diverse set of rocks: foyaites, syenites, and granites. A.G. Vologdin discovered the intrusion in 1924 near the Saibar Mount [50]. This author did not provide a detailed description of the rocks and their relations with each other. Later, other explorers [51–56] described in detail the intrusion with the separation of alkali nepheline syenites and quartz syenites. However, geological data on nepheline syenites were contradictory; G.M.

Saranchina [52] classified them as dykes, and E.E. Fedorov [54] considered them xenoliths in quartz syenites.

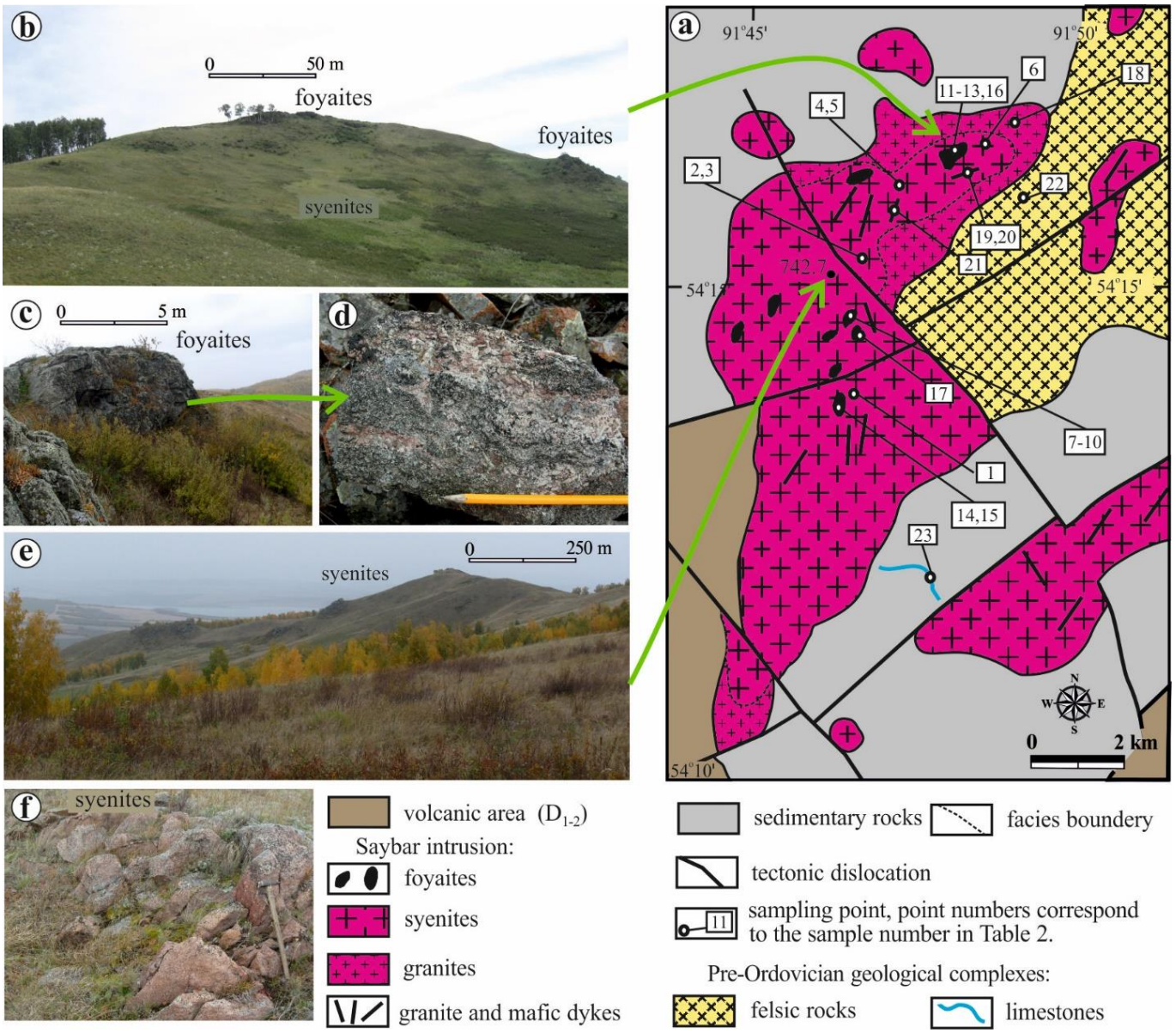

Figure 3. (**a**) Structural geological map of the Saibar intrusion, modified from [49,52–54]. (**b**,**c**) Representative photos showing that foyaite rocks form small outcrops and ridges elevations above syenites. (**d**) Representative photos showing pegmatoid banded nepheline syenites (foyaites) with alternating leucocratic and melanocratic varieties. (**e**) Panorama of the Saibar intrusion at a height of 742.7 m to the north-east. (**f**) Representative photos of rock outcrop with syenites.

The structure of the Saibar intrusion is determined by syenites, connected in places by gradual transitions with foyaites and granites, as well as by dykes of granite and mafic rocks.

Syenites occupy about 90% of the rock mass (Figure 3a,e,f). These are mainly granular rocks. They are subdivided into quartz-free and quartz-bearing varieties. Quartz-free varieties (Figure 4a,b) are dominated by alkali feldspar with numerous crudely perthitic domains composed of twinned albite prevails. Aegirine and arfvedsonite form aggregate of needles. Aegirine is green and brownish-green. In some cases, arfvedsonite replaces aegirine, retaining the octahedral shape of its cross-section, and also yields initially magmatic crystals with hexagonal and rhombic sections. Microcrystals of hornblende, albite,

and biotite are found only in quartz varieties. Accessory minerals are titanite, apatite, and fluorite.

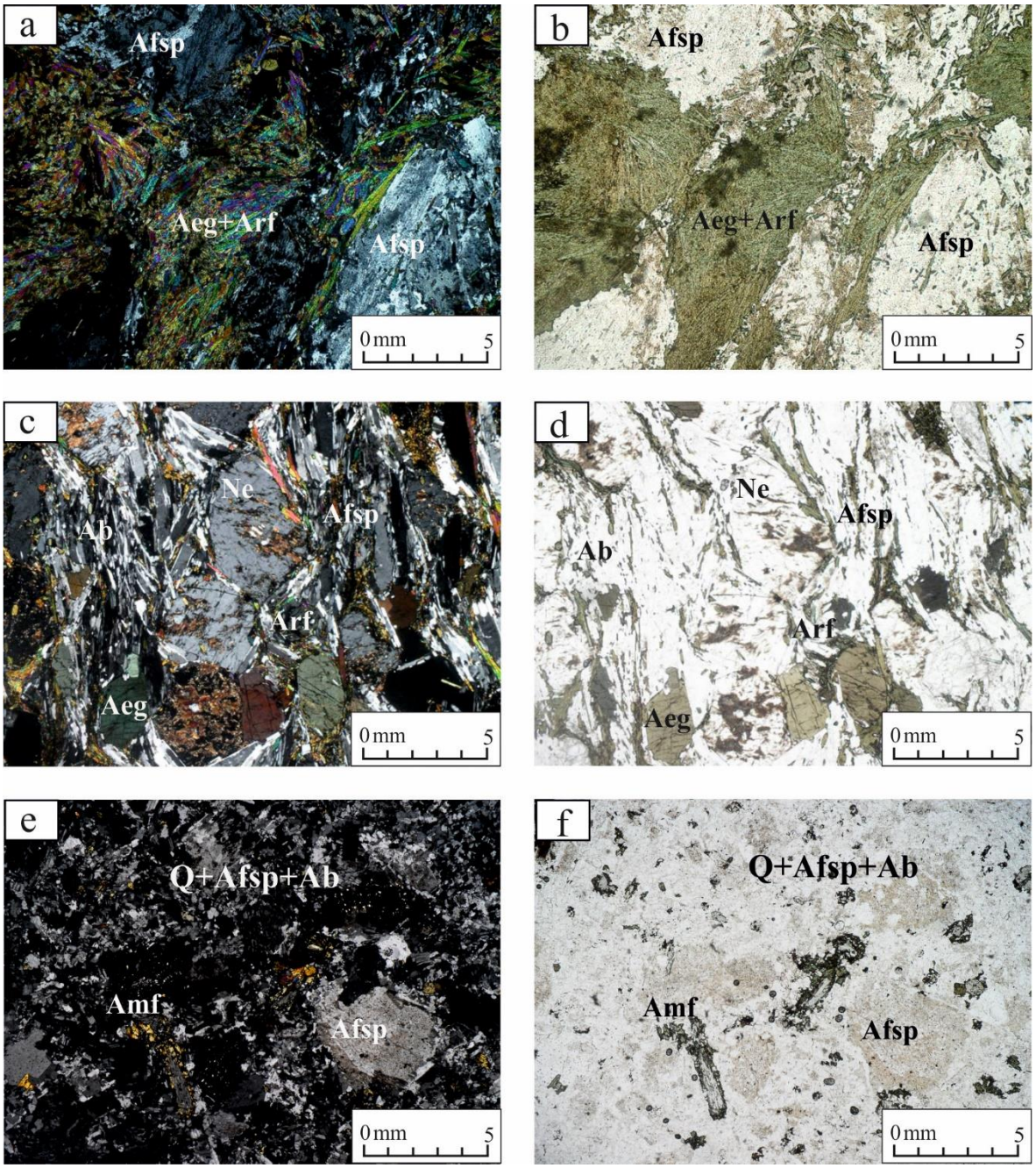

Figure 4. Micro-photos of representative thin sections: (**a**,**b**) quartz-free syenites, alkali feldspar undergoes albitization, aegirine and arfvedsonite form aggregate of needles; (**c**,**d**) foyaites, nepheline forms large crystals and xenomorphic grains between aegirine and alkali feldspar; (**e**,**f**) granites are composed of lamellar alkali feldspar, quartz–alkali feldspar–albite aggregate, and rare amphibole crystals. Left column: crossed polars, right column: parallel polars. Ne = nepheline, Aeg = aegirine, Arf = arfvedsonite, Amf = amphibole, Afsp = alkali feldspar, Ab = albite, Q = quartz.

Nepheline syenites were initially called "saibarites" [55], but in petrographic properties, following the classification in [1], they correspond to foyaites. These rocks comprise separate bodies (from 20 × 50 to 50 × 200 m) connected by gradual transitions with the hosting syenites (Figure 3b). These bodies are found in the northern and central parts of the Saibar intrusion. They morphologically appear as small outcrops and ridges 0.5 to 3 m high (Figure 3c) and have a dyke-like appearance. However, did not discover any clear intrusive

contacts and quenched zones typical of dykes. Foyaites are characterized by variability of petrographic features and gradually transform into syenites. Their texture varies from hypidiomorphic granular to porphyry. Foyaites have melanocratic and leucocratic varieties and banded structures. These are alternating bands with varying ratios of alkali feldspar, albite, aegirine, arfvedsonite, and nepheline. The aegirine-rich bands of 2 to 50 cm thickness wedge out, break off or swell, and grade into irregularly shaped spots (Figure 3d). Aegirine crystals seem aligned in one direction. In places, the bands exhibit coarser fragments containing large (about 1 cm) aegirine and nepheline crystals. Leucocratic foyaites are rich in alkali feldspar and albite. In all foyaite varieties, the alkali feldspar contains perthite with albite exsolutions. Magmatic albite is found as infrequent elongate polysynthetic twins attached to nepheline (Figure 4c,d). Nepheline is hexagonal- and tablet-shaped and commonly replaced by zeolite or analcime, rarely by aggregate of colorless fine-flaked mica. Aegirine forms the sheaf- and felt-like minerals; its color varies from yellowish-green to dark green. Aegirine is always more idiomorphic than arfvedsonite, which is brown and green with a purple (indigo) tint. The bulk mass has a trachytic and hypidiomorphic granular textures defined by various relations of aegirine and albite. Accessory minerals are the same as in nepheline syenites: titanite, apatite, and fluorite.

Granites of the main phase are present as moderately alkaline and alkaline varieties according to [1]. They differ in geological conditions of occurrence and mineral composition. These rocks make up irregular spots varying in size from 10 to 100 m^2 in the endocontact zones in the north and south of the intrusion and are located near the host rocks. Towards the center of the intrusion, they gradually become a coarse-grained quartz variety of syenite. In the endocontact zones, the rocks (Figure 4e,f) have a porphyric structure. Together with plentiful tabular alkali feldspar, they contain quartz–alkali feldspar–albite aggregate and rare amphibole crystals. Granite dykes are 20 m long; their thickness does not exceed 5 m, and that of quenched zones is only a few centimeters. The dykes intrude the Saibar syenites and foyaites, as well as the host rocks [53,54]. Along with alkali feldspar, quartz, and albite, dyke granites contain infrequent grains of aegirine–augite and arfvedsonite along with accumulations of magnetite, accessory apatite, and fluorite on the boundaries. A small number of alkali feldspar crystals have turned gray due to postmagmatic alteration.

Mafic rocks make up infrequent dykes intruding syenites in the central part of the Saibar intrusion. The contact of these dykes with the host rocks is sharp and clear. The dykes are sub-vertical with a predominantly northern strike (350°–30°). The thickness of these dykes varies from 0.2 to 1 m, and their length is 5–15 m. The rock-forming minerals are labradorite and augite. The rocks have a micro-grained ophitic texture. In these rocks, chaotically oriented crystals of labradorite are partially enveloped in augite, which has no rims of its own. Brown tabular hornblende, biotite, and ore minerals are less common. Apatite, titanite, and zircon are typical accessory minerals. The rocks underwent low-temperature hydrothermal alteration, which caused the replacement of labradorite by sericite, mafic minerals by chlorite and epidote, as well as the formation of secondary calcite.

3. Analytical Methods

3.1. Zircon U-Pb Dating

U-Pb dating of zircon was executed at the Institute of Precambrian Geology and Geochronology of the Russian Academy of Sciences, St.-Petersburg, Russia. Zircons were extracted from crushed rock using heavy liquids and magnetic separation techniques. The chemical decomposition of zircons and U-Pb isolation were performed with the conventional technique of T.E. Krogh [57]. The isotope analysis was accomplished with a Finnigan MAT-261 multi-collector mass-spectrometer (Thermo Electron GmbH, Bremen, Germany). The coefficients of fractionation are Pb—0.10% and U—0.08% per atomic unit of mass (a.u.m.). Blank contamination was not more than 0.1 ng Pb and 0.01 ng U. The uncertainties of the measured U/Pb ratios and U and Pb concentrations were 0.8%. Experimental data were processed in the programs PbDAT-1.22 [58] and ISOPLOT-2.10 [59]. In estimating

the ages, the generally accepted values of the decay constants of uranium were used [60]. Corrections for common lead were introduced according to model values [61]. All errors are listed at the 2σ level. Micrographs of zircon were taken on an Ultra 55 scanning electron microscope (accelerating voltage 20 kV) (Carl Zeiss, Oberkochen, Germany).

3.2. Whole-Rock Composition

Samples from the Saibar intrusion were selected for chemical analysis after excluding those that were weathered. Major and trace elements were analyzed at the Institute of Geochemistry (Shared-Use Analytical Center for Isotopic and Geochemistry Studies), Siberian Branch of the Russian Academy of Sciences, Irkutsk, Russia. Major elements were analyzed by XRF with a CPM-25 multichannel spectrometer (Nauchpribor, Orel, Russia), as described by Afonin et al. [62]. Measurements of rare elements were performed using the ICP-MS method on an ELEMENT-2 Finnigan MAT high-resolution mass spectrometer (Thermo Electron GmbH, Bremen, Germany). To address possible matrix effects and to consider instability in the spectra (XRF), the analysts used the internal standard Rh. To calibrate the calculations of elemental contents in ICP-MS measurements, multi-element certified solutions CLMS-1, -2, -4, and SPEX (USA) were applied. Rock samples of mafic composition were prepared by open acid decomposition, and samples of syenites, foyaites, and granites were prepared by fusion with Li-metaborate.

3.3. O-Nd Isotopic Analysis

To perform isotope analysis of oxygen, we collected feldspar samples without any traces of secondary alterations from the Saibar intrusion. These were the fragments weighing 1.5–2.5 mg. They were examined at the Geological Institute, Siberian Branch of Russian Academy of Sciences, Ulan-Ude, Russia, with a Finnigan MAT 253 gas source mass spectrometer (Thermo Electron GmbH, Bremen, Germany) using a double lap system in a classic version (reference sample–sample). To measure $\delta^{18}O$ values, the samples were prepared using laser fluorination with BrF5 reagent employing the technique reported in [63]. The set included the MIR 10–30 facility, and the analyzed minerals were laser heated with CO2 to 1000 °C, and the vacuum main line was used to purify and finally concentrate oxygen. The $\delta^{18}O$ estimates were acquired versus international reference materials NBS-28 (quartz) and NBS-30 (biotite). The internal control was governed by regular measurements of UWG-2 (garnet), inner standard GI-1 (quartz), and Polaris (quartz) from the laboratory at the Institute of Geology of Ore Deposits, Petrography, Mineralogy and Geochemistry, Russian Academy of Sciences, Moscow, Russia. The error of obtained $\delta^{18}O$ values was at the level (1σ) ± 0.2‰. Representative samples were selected for Sm-Nd analysis, which was performed at the Institute of Geochemistry (Shared-Use Analytical Center for Isotopic and Geochemistry Studies), Siberian Branch of Russian Academy of Sciences, Irkutsk, Russia. About 100 mg of the whole-rock powder was dissolved in the mixture of HF, HNO_3, and $HClO_4$. Before dissolution, ^{149}Sm–^{150}Nd spike solution was added to all samples. The REEs were separated on BioRad AGW50-X8 200–400 mesh resin using conventional cation exchange techniques [64–66]. Sm and Nd were separated by extraction chromatography with LN-Spec (100–150 mesh) resin [67]. During the measurement, total blanks were 0.1–0.2 ng for Sm and 0.2–0.5 ng for Nd.

Isotopic compositions of Sm and Nd were determined on a NEPTUNE Plus Multi-Collector ICP-MS (Thermo Electron GmbH, Bremen, Germany) in static mode. The precision (2σ) of Sm and Nd contents and $^{147}Sm/^{144}Nd$ ratios was ±0.4% and ±0.003% for $^{143}Nd/^{144}Nd$ ratios. The $^{143}Nd/^{144}Nd$ ratios were normalized against $^{146}Nd/^{144}Nd = 0.7219$. The results of the international standards are: (1) JNdi-1 (n = 40), $^{143}Nd/^{144}Nd = 0.512107 \pm 4$ (recommended value, $^{143}Nd/^{144}Nd = 0.512115 \pm 7$ [68]); (2) BCR-2 (n = 28), $^{143}Nd/^{144}Nd = 0.512630 \pm 14$; Nd = 28.77 ± 0.13 ppm; Sm = 6.52 ± 0.03 ppm; (3) AGV-2 (n = 8), $^{143}Nd/^{144}Nd = 0.512769 \pm 16$; Nd = 30.3 ± 0.02 ppm; Sm = 5.42 ±0.03 ppm.

4. Results

4.1. Zircon U-Pb Geochronology

To identify the time of the Saibar intrusion formation in the central part of the intrusion, we collected a bulk sample (20 kg) of melanocratic foyaites (sample 73–99), from which four fractions of zircons varying in coloring were analyzed. From these samples, by means of optical microscopy in transmitted light with the use of immersion liquids, non-zoned translucent brown and colorless zircons were selected without inclusions, which could be considered "ancient cores". The crystals have dipyrimid shape with developed prism sides (Figure 5). The translucent brown crystal is primarily short columnar or isometric with elongation of 1.0–1.3. Colorless zircons include some grains with elongation of 1.5–2.5. The morphological and crystallographic features of zircon indicate its magmatic nature.

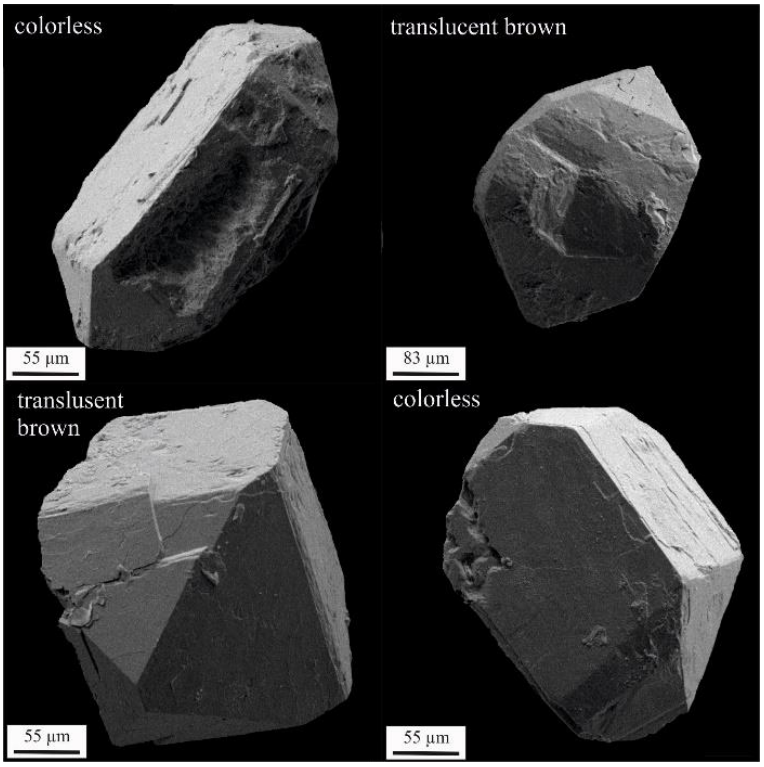

Figure 5. Photomicrography of selected zircon crystals from melanocratic foyaite (sample 73–99). The morphology of zircon grains is defined by the combination of a dipyramid and a prism, which indicates their magmatic origin.

The results of U-Pb isotope analysis for melanocratic foyaites of the central site are shown in Table 1 and Figure 6. Fraction 1 zircon contains an insignificant amount of U (24.2 ppm) and has a slight inverse age-related discordance. The U content in grains of fractions 2, 3, and 4 exceeds 1000 ppm, and their ages have a direct age sequence $t(^{206}Pb/^{238}U) < t(^{207}Pb/^{235}U) < t(^{207}Pb/^{206}Pb)$. The isochron built from points 2, 3, and 4 comes through the beginning of coordinates (22 ± 6 Ma) and crosses the concordia in the point of age value 457 ± 10 Ma, and the mean squared weighted deviation (MSWD) is 0.14. Considering that melanocratic foyaites gradually transform into syenites and are therefore coeval, we infer that the obtained dating corresponds to the age of the Saibar intrusion.

Table 1. U-Pb isotopic data for the Saibar intrusion.

№	Weight (mg)	Pb, ppm	U, ppm	$^{206}Pb^{a}/^{204}Pb$	$^{207}Pb^{b}/^{206}Pb$	$^{208}Pb^{b}/^{206}Pb$	$^{206}Pb/^{238}U$	$^{207}Pb/^{235}U$	$^{206}Pb/^{238}U$	$^{207}Pb/^{235}U$	$^{207}Pb/^{206}Pb$
				Isotope Ratios					Age, Million Years		
Samples 73–99, Melanocratic Foyaite											
1	0.40	2.05	24.2	1550	0.054314 ± 168	0.27435 ± 85	0.07170 ± 9	0.5370 ± 18	446.4 ± 3.6	436.4 ± 4.4	384.1 ± 7.7
2	2.33	109	1255	546.5	0.056033 ± 31	0.29725 ± 17	0.06786 ± 10	0.5243 ± 8	423.3 ± 3.3	428.0 ± 4.3	453.7 ± 9.0
3	4.86	88	1095	3068	0.056116 ± 24	0.25625 ± 11	0.06987 ± 9	0.5406 ± 7	435.4 ± 3.5	438.8 ± 4.4	456.9 ± 9.1
4	1.48	148	2100	1677	0.056000 ± 22	0.29441 ± 12	0.05862 ± 8	0.4526 ± 6	367.2 ± 2.9	379.1 ± 3.8	452.5 ± 9.0

Notes: a—isotope ratios corrected for fractionation and blank; b—isotope ratios corrected for fractionation, blank and common lead. Errors in age values at the 2σ level were calculated based on the results of parallel age determinations of standard TNA-16 zircon.

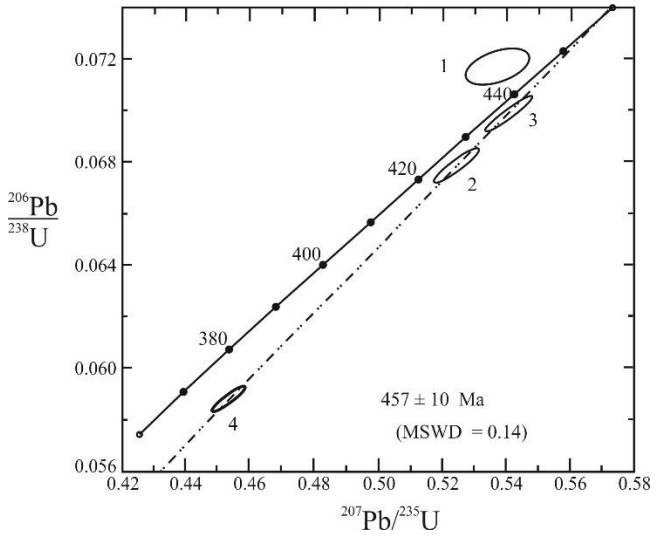

Figure 6. U-Pb dating results and concordia diagrams for melanocratic foyaites of the Saibar intrusion.

4.2. Major and Trace Element Geochemistry

Table 2 shows the chemical compositions of the Saibar intrusive rocks. Syenites are characterized by SiO_2 values from 61.52 to 66.39 wt.%, total alkalinity ($Na_2O + K_2O$) from 8.92 to 11.63 wt.%, and agpaite coefficients less than 1. All foyaites differ from syenites in high alkali contents ($Na_2O + K_2O$ = 12.27–13.95 wt.%), which is reflected in the appearance of modal nepheline. Variations in SiO2 are noted in the range from 53.91 to 61.64 wt.%, which corresponds to the compositions of foid syenites, on the classification TAS diagram (Figure 7a; [69]). The average SiO_2 content in melanocratic foyaites is 57.41 wt.%; in leucocratic 59.14 wt.%, the agpaite coefficient varies from 0.97 to 1.30 and does not depend on the melanocratic degree of the foyaites. In the TAS diagram (Figure 8), the points of their composition are located in the syenite field and at the boundaries of the syenite–alkaline syenite and syenite–alkaline granite or granosyenite fields [69]. All granites are similar in SiO_2 content (68.75–69.93 wt.%) but differ in total alkalinity. Dyke granites are characterized by $Na_2O + K_2O$ in the range from 10.24 to 10.91 wt.%, with variations of the agpaite coefficient from 0.95 to 1.01 (A.C., Table 2). The granite of the endocontact zone is characterized by the sum $Na_2O + K_2O$ of 9.09 and the agpaite coefficient of 0.82. SiO_2 content of mafic dykes varies from 61.52 to 66.39 wt.%; the total $Na_2O + K_2O$ is from 10.24 to 10.91 wt.%, which corresponds to the monzogabbrodiorite composition [69].

Table 2. Chemical composition of the Saibar rocks.

Number	1	2	3	4	5	6	7	8
Sample	**SBR 4/6**	**SBR 1/5**	**SBR 1/7**	**SBR 3/1**	**SBR 3/3**	**SBR 4/4**	**MSK 1/1**	**MSK 1/2**
Rock Type	**Syenites**						**Leucocratic Foyaites**	
				Major Elements (wt.%)				
SiO_2	63.68	61.52	64.02	63.86	66.39	65.21	57.62	61.64
TiO_2	0.54	1.00	0.70	1.11	0.57	0.73	1.25	1.03
Al_2O_3	16.72	15.95	17.17	16.53	16.40	16.80	15.57	17.79
TFe_2O_3	3.35	10.26	6.57	5.34	3.71	4.39	7.22	5.73
MnO	0.13	0.43	0.28	0.25	0.12	0.20	0.30	0.27
MgO	0.71	0.36	0.37	0.48	0.50	0.07	1.28	0.11
CaO	1.71	0.11	0.25	0.48	0.83	0.50	1.86	0.20
Na_2O	7.31	4.48	5.71	6.66	6.57	6.87	8.83	7.89
K_2O	5.41	4.44	4.25	4.97	4.63	4.48	4.22	4.89
P_2O_5	0.13	0.04	0.07	0.10	0.11	0.18	0.14	0.06
LOI	0.66	1.43	0.65	0.71	0.52	0.93	1.96	0.54
Total	100.35	100.02	100.04	100.49	100.35	100.36	100.25	100.15
#Mg	33.1	7.5	11.5	17.4	24.0	3.6	29.3	4.3
A.C.	1.07	0.76	0.82	0.99	0.96	0.96	1.23	1.03
A/CNK	0.80	1.29	1.19	0.96	0.95	0.98	0.69	0.95
A/NK	0.93	1.31	1.23	1.01	1.04	1.04	0.82	0.97
$Na_2O + K_2O$	12.72	8.92	9.96	11.62	11.20	11.35	13.05	12.78
MALI	11.01	8.82	9.71	11.14	10.37	10.85	11.19	12.58
				Trace Elements (ppm)				
Rb	175	174	125	153	148	151	175	131
Ba	670	346	390	407	615	390	532	196
Th	10.3	17.6	8.9	22.2	33.1	55.9	20.7	26.6
U	3.07	6.00	5.12	4.73	6.61	9.35	7.27	6.02
Nb	30.1	38.6	64.1	91.3	63.0	105.1	82.6	74.0
Ta	1.83	1.23	3.80	6.01	3.50	5.28	2.82	3.08
La	69.6	46.5	58.1	87.7	90.9	183.0	223.2	78.6
Ce	128.5	102.3	136.8	197.1	169.7	336.5	495.1	155.3
Pb	10.9	29.1	23.7	42.9	29.3	30.8	44.1	42.1
Pr	14.04	8.26	15.86	23.32	16.85	32.15	54.18	15.41
Sr	286	26	65	84	168	103	232	72
Nd	46.8	26.5	54.9	81.4	55.9	99.9	186.0	51.0
Zr	384	1065	996	1181	1285	880	940	1257
Hf	10.03	27.76	23.51	26.04	26.16	20.51	18.84	26.48
Sm	7.86	4.53	9.11	13.37	9.54	17.10	31.56	8.99
Eu	1.48	0.79	1.58	2.35	1.43	3.15	5.53	1.59
Gd	7.29	3.88	7.50	11.59	8.51	17.40	27.30	8.23
Tb	0.98	0.69	1.26	1.84	1.28	2.79	3.86	1.50
Dy	6.44	4.51	8.36	11.19	8.06	19.47	24.57	9.88
Y	38.3	35.8	47.1	59.4	53.4	138.0	123.7	71.3
Ho	1.30	1.04	1.84	2.38	1.78	4.55	4.68	2.24
Er	3.96	3.70	5.95	7.95	6.22	15.40	13.80	7.93
Tm	0.64	0.64	1.03	1.28	1.01	2.58	1.98	1.33
Yb	4.50	5.86	7.68	9.79	7.69	17.95	13.12	10.36
Lu	0.79	1.18	1.30	1.61	1.28	2.78	1.97	1.71
ΣLREE	258.9	183.6	265.7	389.5	333.4	651.6	958.5	300.3
ΣMREE	24.1	14.4	27.8	40.3	28.8	59.9	92.8	30.2
ΣHREE	11.2	12.4	17.8	23.0	18.0	43.3	35.6	23.6
$(La/Yb)_n$	10.6	5.4	5.2	6.1	8.1	7.0	11.7	5.2
Eu*	0.59	0.57	0.57	0.57	0.48	0.56	0.57	0.56

Table 2. *Cont.*

	9	10	11	12	13	14	15	16
	MSK 1/3	**MSK 1/5**	**SBR 1/1**	**SBR 1/2**	**SBR 1/3**	**SBR 4/7**	**SBR 4/8**	**SBR 3/2**
	Leucocratic Foyaites		**Melanocratic Foyaites**					
				Major Elements (wt.%)				
SiO_2	56.94	60.37	56.09	53.91	57.45	60.17	58.10	58.72
TiO_2	0.86	0.88	0.63	0.83	0.76	0.85	0.74	1.12
Al_2O_3	18.12	16.03	17.36	15.93	18.54	16.86	19.40	17.47
TFe_2O_3	5.13	5.07	8.55	11.27	7.03	5.31	3.52	6.21
MnO	0.25	0.26	0.20	0.26	0.26	0.32	0.26	0.33
MgO	0.53	1.01	0.46	0.42	0.85	0.61	0.77	0.78
CaO	2.30	1.83	1.21	1.19	0.70	1.26	1.33	0.90
Na_2O	7.69	8.08	8.89	9.93	7.45	8.22	9.05	7.26
K_2O	5.13	5.36	4.76	4.00	5.36	5.08	4.90	5.01
P_2O_5	0.04	0.19	0.02	0.04	0.02	0.09	0.13	0.07
LOI	2.85	0.92	1.88	2.48	1.13	1.58	2.18	1.11
Total	99.84	100.00	100.05	100.26	99.55	100.35	100.38	98.98
#Mg	19.4	31.6	11.2	7.9	22.0	21.1	33.8	22.7
A.C.	1.00	1.19	1.14	1.30	0.97	1.13	1.04	0.99
A/CNK	0.81	0.71	0.79	0.70	0.96	0.79	0.86	0.92
A/NK	1.00	0.84	0.88	0.77	1.03	0.89	0.96	1.01
$Na_2O + K_2O$	12.82	13.44	13.65	13.93	12.81	13.30	13.95	12.27
MALI	10.52	11.61	12.45	12.74	12.11	12.04	12.62	11.37
				Trace Elements (ppm)				
Rb	190	178	339	320	365	199	195	181
Ba	362	459	159	125	204	338	222	490
Th	25.0	22.0	14.4	29.4	10.2	32.3	21.0	20.7
U	7.04	8.25	4.38	13.95	3.71	13.42	8.86	5.33
Nb	44.6	68.1	22.8	56.6	29.6	63.0	59.0	68.4
Ta	1.33	4.36	0.86	1.74	1.04	1.60	2.34	3.32
La	103.0	126.2	39.6	112.3	35.2	82.1	98.3	81.6
Ce	194.1	273.5	65.5	195.3	61.9	130.7	162.5	155.4
Pb	48.6	20.7	22.1	47.2	17.4	68.0	35.7	47.9
Pr	19.99	27.49	6.23	17.15	5.89	11.83	15.76	15.84
Sr	991	190	169	98	76	165	182	156
Nd	66.7	93.7	19.0	49.9	18.7	35.4	49.5	51.2
Zr	779	899	1053	1533	839	1181	735	1272
Hf	16.12	20.14	26.73	40.12	18.56	26.97	15.27	27.18
Sm	11.35	15.66	2.90	7.78	3.36	5.81	7.34	8.60
Eu	1.95	2.51	0.50	1.36	0.59	1.10	1.19	1.54
Gd	9.38	12.67	2.29	7.82	3.31	6.10	6.80	8.44
Tb	1.49	1.99	0.34	1.12	0.46	0.99	0.93	1.43
Dy	10.25	12.31	2.27	6.74	3.09	7.74	6.41	10.33
Y	59.4	73.7	14.2	41.8	20.5	65.6	52.6	70.8
Ho	2.08	2.57	0.53	1.41	0.70	1.94	1.55	2.47
Er	6.52	8.06	1.97	4.92	2.65	7.20	5.39	9.25
Tm	0.99	1.23	0.42	0.94	0.53	1.32	0.97	1.57
Yb	7.14	8.58	4.25	8.71	4.92	9.95	7.26	12.35
Lu	1.19	1.38	0.98	1.71	0.99	1.73	1.24	1.96
ΣLREE	383.8	520.9	130.3	374.7	121.7	260.0	326.1	304.0
ΣMREE	34.4	45.1	8.3	24.8	10.8	21.7	22.7	30.3
ΣHREE	17.9	21.8	8.2	17.7	9.8	22.1	16.4	27.6
$(La/Yb)_n$	9.9	10.1	6.4	8.8	4.9	5.7	9.3	4.5
Eu*	0.56	0.53	0.58	0.53	0.54	0.57	0.51	0.55

Table 2. *Cont.*

	17	18	19	20	21	22	23	24
	73–99	SBR 1/4	SBR 4/1	SBR 4/3	SBR 4/9	SBR 4/17	SBR 4/14	
	Melanocratic Foyaites	Granite of Main Phase	Granites of Dykes		Mafic Dyke	Host Felsic Rock	Host Limestone	Hybrid Melt
					Major Elements (wt.%)			
SiO_2	52.71	69.93	68.75	68.94	51.08	66.30	0.1	59.40
TiO_2	1.87	0.43	0.39	0.39	0.87	0.33	0.01	1.03
Al_2O_3	15.92	14.91	14.96	15.12	15.50	18.38	0.15	15.38
TFe_2O_3	8.73	2.92	2.75	3.04	7.58	1.53	<0.5	
MnO	0.64	0.08	0.18	0.09	0.11	0.03	0.01	0.23
MgO	1.37	0.59	0.05	0.37	7.96	0.17	0.39	0.47
CaO	3.55	1.07	1.52	0.53	7.20	0.59	59.1	4.58
Na_2O	7.79	4.34	5.64	6.28	4.21	7.58	<0.1	
K_2O	3.06	4.75	4.60	4.63	1.66	5.22	0.04	4.62
P_2O_5	0.05	0.09	0.26	0.32	0.24	0.05	0.02	0.09
LOI	3.99	0.60	1.29	0.70	3.89	0.29	39.77	3.44
Total	99.68	99.71	100.39	100.41	100.30	100.47	99.59	100.43
#Mg	26.8	31.9	4.1	22.1	71.0	20.6		
A.C.	1.23	0.82	0.95	1.01	0.56	0.99		
A/CNK	0.70	1.05	0.88	0.93	0.71	0.96		
A/NK	0.99	1.21	1.05	0.99	1.78	1.01		
$Na_2O + K_2O$	10.85	9.09	10.24	10.91	5.87	12.80		
MALI	7.30	8.02	8.72	10.38	−1.33	12.21		
					Trace Elements (ppm)			
Rb	116	158	204	186	54	57	0.86	142.35
Ba	265	612	541	279	953	229	17.5	379.7
Th	16.2	27.4	76.3	47.8	1.0	3.7	0.1	20.6
U	7.08	5.37	5.76	8.17	0.71	0.99	0.79	4.45
Nb		46.0	61.1	59.5	4.9	10.9	0.16	84.92
Ta	4.06	3.85	3.78	3.31	0.29	0.67		
La	79.3	53.3	224.8	424.7	17.0	13.8	0.42	81.59
Ce	154.1	111.5	490.4	750.0	36.0	38.5	0.78	183.36
Pb		25.7	16.9	16.9	2.5	11.7	1.15	39.98
Pr		11.57	47.96	79.46	4.48	5.48	0.14	21.70
Sr	925	201	128	132	901	36	335	101
Nd	58.1	38.9	160.8	248.6	18.6	21.9	0.54	75.74
Zr		254	354	305	124	49	3.8	1098
Hf	22.13	7.57	9.86	8.38	3.02	1.65	0.05	24.22
Sm	10.37	7.00	34.80	45.20	4.03	4.27	0.08	12.44
Eu	1.84	1.06	6.74	8.33	1.51	0.96	0.03	2.19
Gd	7.59	5.31	40.04	46.09	4.69	3.57	0.11	10.79
Tb	1.47	0.88	8.15	7.84	0.58	0.49	0.01	1.71
Dy		5.28	63.00	54.99	3.47	3.06	0.09	10.41
Y		33.0	479.9	423.4	18.7	16.3	0.67	55.29
Ho		1.13	15.52	12.85	0.69	0.63	0.02	2.21
Er		3.76	53.57	42.05	2.01	1.67		
Tm	1.10	0.61	8.41	6.59	0.28	0.27	0.01	1.19
Yb	8.18	4.57	52.61	39.72	1.80	1.62	0.05	9.11
Lu	1.41	0.67	7.25	5.28	0.27	0.25	0.01	1.50
ΣLREE		215.3	924.0	1502.8	76.1	79.7		
ΣMREE		19.5	152.7	162.5	14.3	12.4		
ΣHREE		10.7	137.4	106.5	5.1	4.4		
(La/Yb)n	6.6	8.0	2.9	7.3	1.3	5.8		
Eu*	0.60	0.52	0.56	0.56	1.07	0.74		

Notes: LOI = loss on ignition; TFe_2O_3 = Total Fe calculated as Fe_2O_3; A/CNK = $Al_2O_3/(CaO + Na_2O + K_2O)$ (mol.%); A/NK = $Al_2O_3/(Na_2O + K_2O)$ (mol.%); MALI = $Na_2O + K_2O$–CaO (mol.%), agpaite coefficient (A.C.) = $(Na_2O + K_2O)/Al_2O_3$ (with molar ratio), Eu* = $Eu_n/((Sm_n + Gd_n)/2)$. Light rare earth elements (LREEs)—La, Ce, Pr, Nd; middle rare earth elements (MREEs)—Sm, Eu, Gd, Tb, Dy; heavy rare earth elements (HREEs)—Ho, Er, Tm, Yb, Lu. Empty values indicate no measurements. Na_2O and TFe_2O_3 values for limestones are less than the detection limit. The composition of the hybrid melt (HM) was calculated for each element using the following formula: HM = (concentration of an element in the sample SBR 3/1 × 0.93) + (concentration of an element in the sample SBR 4/14 × 0.07).

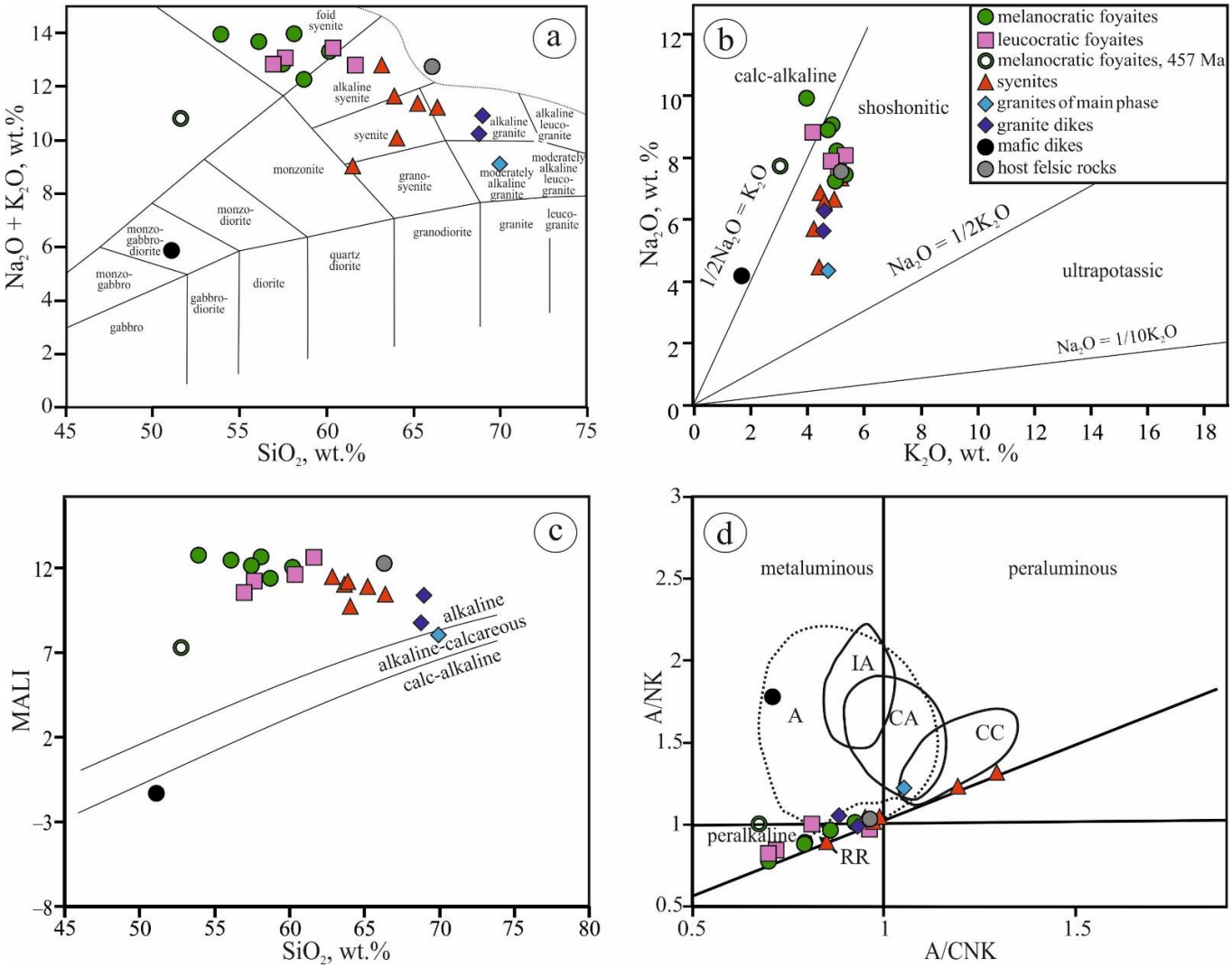

Figure 7. Major element classification of the Saibar rocks. (**a**) Total alkali vs. silica (TAS) diagram [69]; (**b**) Na_2O vs. K_2O alkalinity diagram; (**c**) MALI ($Na_2O + K_2O - CaO$) vs. SiO_2 diagram. (**d**) A/NK vs. A/CNK diagram. Island arc (IA), continental arc (CA), continental collision (CC), rift-related (RR), and anorogenic (A) granite fields are taken from [70].

All samples show different enrichment in K_2O content and Na_2O/K_2O ratios (Figure 7b); with a decrease in SiO_2 content among all Saibar rocks, the composition points shift from shoshonitic to calc–alkaline composition field. The modified alkali–lime index (MALI) obtained from the $Na_2O + K_2O - CaO$ vs. SiO_2 plot (Figure 7c) is strongly alkaline for foyaites and syenites and is associated with the enrichment by albite and alkali feldspar. The composition point of the mafic dyke is plotted in the calc–alkaline field.

Foyaite samples have metaluminous (A/CNK = 0.69–0.95) values. Compared to foyaites, syenites and granites are intermediate in composition between oversaturated alkalis and peraluminous ones (A/CNK in syenites = 0.95–1.29, A/CNK in granites = 0.88–1.05; Figure 7d). These intermediate metaluminous–peraluminous and alkaline characteristics are typical for syenites in continental settings [70,71].

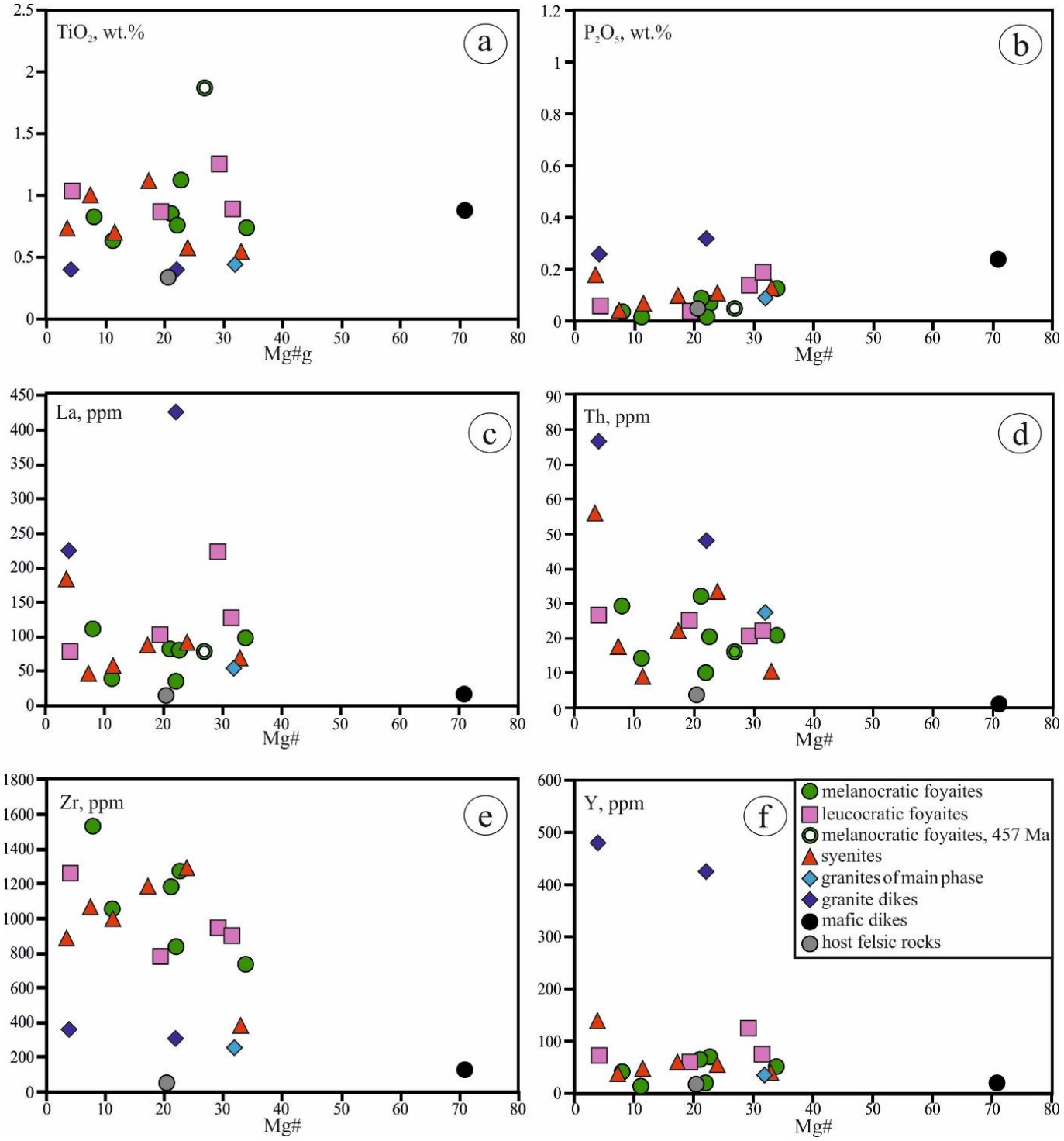

Figure 8. (**a**–**f**) Variations of TiO_2, P_2O_5, La, Th, Zr, and Y vs. Mg# for the Saibar rocks. Mg# = Mg × 100/(Mg + Fe^{2+}), where Mg = MgO/40.31, Fe^{2+} = (Fe_2O_3* × 0.8998 × 0.85)/71.85.

The rocks comprising the main volume of the intrusion exhibited high total Fe, calculated as Fe_2O_3, and low MgO contents; the Mg# value varies in foyaites from 4 to 34 and in syenites from 3.5 to 24, and in granite Mg# corresponds to 32. In dyke granites Mg# varies from 4 to 22 (Table 2). These variations indicate a high degree of fractionation of the initial magmas and practically do not affect the change in the concentrations of both major components (SiO_2, P_2O_5, TiO_2) and trace elements (La, Th, Zr, and Y; Figure 8a–f). Compared to these granites, foyaites and syenites have the highest TiO_2 (0.6–1.3 wt.%)

and Zr (700–1550 ppm) contents. In all granite compositions, Zr is about 300 ppm. Dyke granites are enriched in P_2O_5, La, Th, and Y compared to other granites. Mafic dykes are characterized by high Mg# value (71). These rocks are enriched in P_2O_5 but exhibit depleted La, Th, and Zr compared to other rock types of the Saibar intrusion.

A wide range of ΣREE is typical for all samples: syenites (210–755 ppm), foyaites (142–1087 ppm), and granites (246–1771 ppm). The REE spectra normalized to chondrite [72] and spidergram normalized to primitive mantle [72] show a great similarity in the rock compositions of the Saibar intrusion (Figure 9). These rocks are geochemically close to A-type granites [73], which are characterized by enrichment in high field strength elements (HFSEs) and heavy rare earth elements (HREEs) in combination with low Sr and Ti concentrations, which is reflected in a spidergram. All rocks comprising the main volume of the Saibar intrusion demonstrate enrichment in light rare earth element (LREE) concentrations ($(La/Sm)_n$ = 4–9), weakly fractionated REE patterns, almost horizontal distribution in the medium rare elements (MREEs) as well as HREEs ($(Dy/Yb)_n$ = 0.35–1.23; $(Sm/Yb)_n$ = 0.63–2.62), and moderate negative Eu anomalies (Eu* = 0.48–0.60). These rocks have generally positive Rb, Th, U and negative Ba, Sr, P, Ti anomalies. Dyke granites differ from syenites and foyaites in the presence of a negative Zr-Hf anomaly. The nature of these differences may be associated with the fractionation of zirconium during the formation of granite dykes.

Syenites and granites of the main phase have a similar distribution of REE patterns (Figure 9a,b). Dyke granites (samples SBR 4/1 and SBR 4/3) and granites of main phases (sample SBR 1/4) differ according to geochemical data. Dyke granites are characterized by negative Nb, Ta, Zr, Hf, and Ti anomalies (Figure 9c,d) with significantly higher ΣREE concentration than in syenites. Granites of the main phase are distinguished by a lower content of total alkalinity and a higher potassium composition (K_2O/Na_2O = 1.1) in comparison with dyke granites (Table 2; Figure 7a,b). The Nb, Ta, Zr, Hf anomalies are practically absent, the Ti anomaly is weakly expressed in granites of the main phase, and in terms of the content of incompatible elements, these granites are close to the most primitive syenite with low ΣREE concentrations.

Foyaites differ in the level of MREE enrichment as ΣREE increases. Melanocratic foyaites are characterized by a marked deflection in the MREE and HREE ($(Dy/Yb)_n$ = 0.41–0.58) concentrations; leucocratic foyaites have a subhorizontal distribution of MREE and HREE patterns ($(Dy/Yb)_n$ = 0.51–0.71). All foyaites are relatively enriched in almost the entire spectrum of incompatible elements. In terms of geochemical characteristics, the compositions of syenites completely overlap with those of foyaites (Figure 9e,f). Mafic dykes differ from syenites and foyaites because geochemically they exhibit depleted LREEs, HREEs, Rb, Th, U, K, Nb, Ta, Zr, Hf and are enriched in Ba, P concentrations.

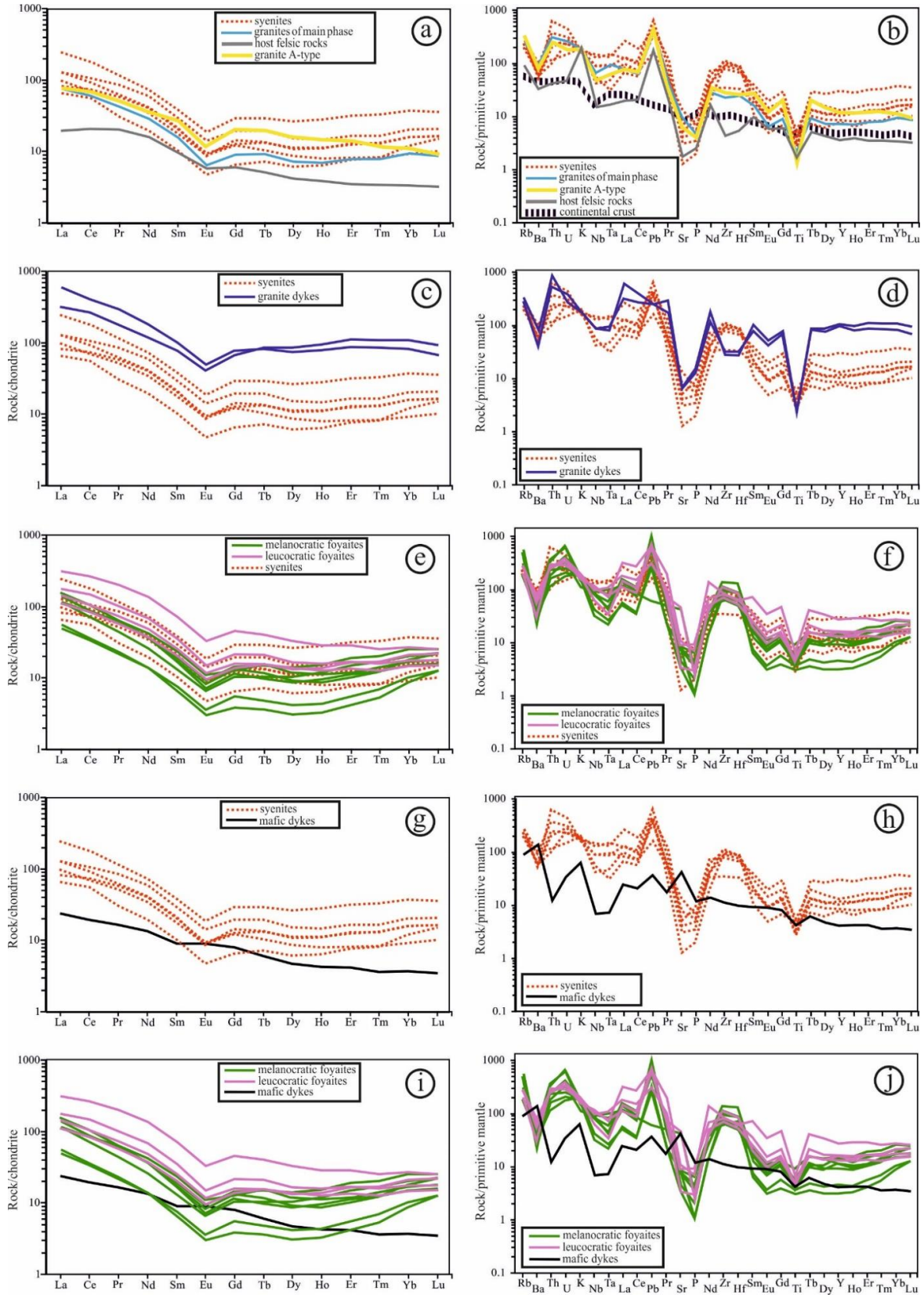

Figure 9. (**a**–**j**) REE diagram, normalized to chondrite [72], and spidergram, normalized to primitive mantle [72], for the Saibar rocks. The figure illustrates that leucocratic foyaites are enriched in LREEs and MREEs in comparison with the melanocratic foyaites. Dyke granites are enriched in Th, U, and REEs in comparison with granites of the main phase. Syenites are similar in geochemical characteristics to foyaites. A-type (anorogenic) granites are from [73]. Continental crust is from [74].

4.3. O-Nd Isotopes

The oxygen isotopic composition was analyzed in alkali feldspars of syenite, foyaite, and granite (Table 3). The $\delta^{18}O$ values vary over a wide range (6.3–10.2‰). In the composition range from foyaites to syenites and granites, as SiO_2 increases, enrichment in the heavy oxygen isotope occurs (Figure 10a).

Table 3. $\delta^{18}O$,‰ in alkali feldspars and Sm-Nd isotope compositions in the Saibar rocks.

Number	Sample	Sm, ppm	Nd, ppm	$^{147}Sm/^{144}Nd$	$^{143}Nd/^{144}Nd$	ε(T)	Age, Ma	$\delta^{18}O$,‰
Syenites								
2	SBR 1/5	4.28	25.52	0.10215	0.51257	4.1	457	10.8
3	SBR 1/7	8.23	49.51	0.10124	0.51261	4.9	457	10.7
4	SBR 3/1							10.6
5	SBR 3/3	8.44	52.54	0.09786	0.5126	5	457	9.3
Leucocratic Foyaites								
7	MSK 1/1							6.5
8	MSK 1/2							10.2
9	MSK 1/3							6.9
10	MSK 1/5							7.8
Melanocratic Foyaites								
11	SBR 1/1	2.47	15.7	0.09593	0.51258	4.8	457	8.2
12	SBR 1/2	6.7	42.44	0.09616	0.51256	4.3	457	7.1
13	SBR 1/3							6.3
16	SBR 3/2							7.6
Granite of the Main Phase								
18	SBR 1/4	6.32	38.34	0.10036	0.51256	4.1	457	10.5
Dyke Granites								
20	SBR 4/3	27.28	233	0.07047	0.512492	4.5	457	

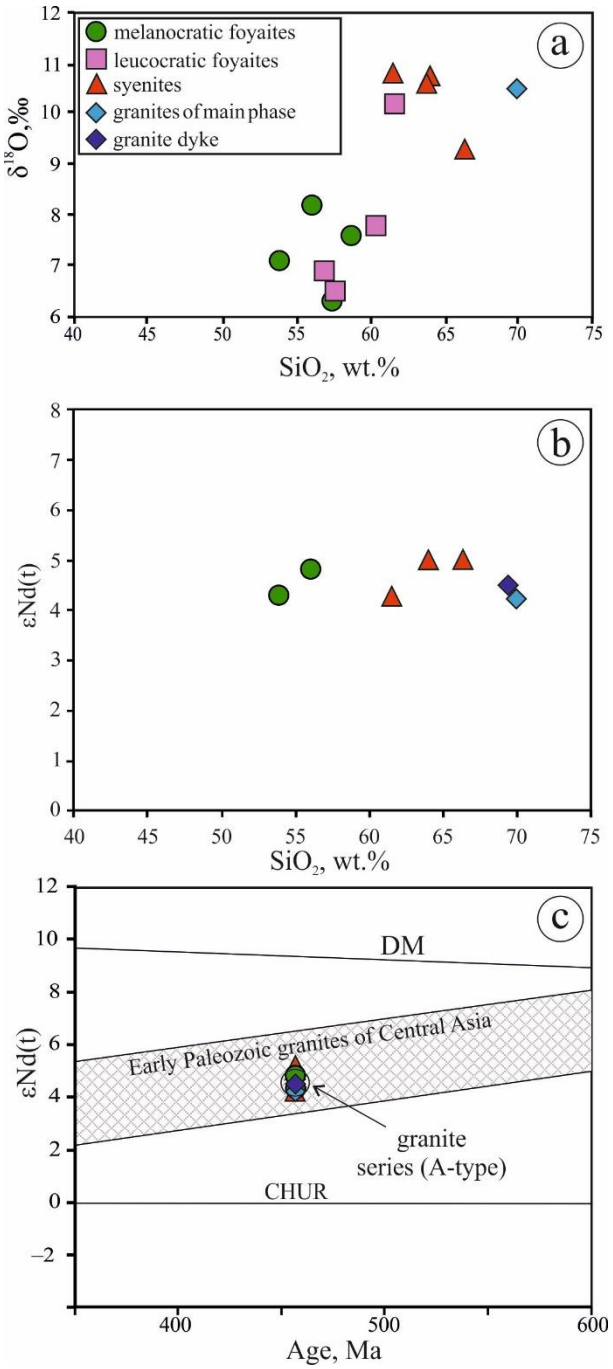

Figure 10. (**a**) $\delta^{18}O$ (‰) vs. SiO_2 (wt.%) diagram for the studied alkali feldspars; (**b**) εNd(t) vs. SiO_2 (wt.%) diagram; and (**c**) εNd(t) vs. age (Ma) diagram for the Saibar rocks in comparison with granite series (A-type) of the Kuznetsk Alatau and Batenevskiy Ridge of the Altay-Sayan fold belt [48] and the Early Paleozoic granites of Central Asia [75–77].

The Nd isotopic composition was investigated in two samples of melanocratic foyaites, three samples of syenites, and two samples of granites (Table 3). εNd(t) values were calculated using the U-Pb age of zircon (457 Ma) obtained from the study of melanocratic foyaites. All samples are characterized by positive εNd(t) values from +4.1 to +5.0. The narrow range of εNd(t) values in the Saibar rocks characterizes a homogeneous magma source. The εNd(t) values in the analyzed samples do not correlate with the SiO_2 content (Figure 10b).

5. Discussion

5.1. Parent Magmas and Petrogenesis

The following important geological observations make it possible to assess the composition of parent magmas and the evolutionary patterns of rock compositions using geochemical and isotopic data. Note that the formation of the intrusion was accompanied by at least two phases of injection. The formation began with the injection of large volumes of magmas, which served as the parent magma for syenites of the first (main) phase. In some cases, these rocks pass into foyaites, forming a continuous row: quartz syenites–quartz-free syenites–nepheline syenites (foyaites). In the marginal parts of the main intrusive phase, corresponding to the endocontact zone, quartz syenites transformed into granites. Later (second phase), syenites of the intrusive were penetrated by rare dykes of granites and mafic rocks, which do not intersect with each other.

Within the Saibar intrusion, there are no mafic rocks with a SiO_2 content of less than 52 wt.% that preceded or accompanied the formation of syenites. This limits the possibility of reconstructing the composition of magmas that was parental for the syenitic rocks. At the same time, the other syenite-bearing intrusions of the Altai-Sayan fold belt contain mafic rocks formed synchronously with examined syenites, which indicates their correspondence to the composition of parent magmas [32–45]. Accordingly, the geological affinity of the Saibar intrusion to other similar intrusions suggests a genetic connection between its rocks and the mafic magmas, which occurred at levels of the magmatic system inaccessible to observation. Mafic dykes of the Saibar intrusion occurred after the formation of the main intrusion phase; therefore, we have no reason to classify them as rocks corresponding to the composition of the parent magmas.

Accordingly, we considered the part of the magmatic evolution of the initial magmas, which corresponds to syenites, foyaites, and all varieties of felsic rocks.

We found that the main intrusive phase contains a forbidden association of quartz-bearing rocks and nepheline-bearing rocks. The points of the modal compositions of these rocks, calculated by the CIPW method, are subdivided in the Ne-Di-Q triangle diagram (Figure 11).

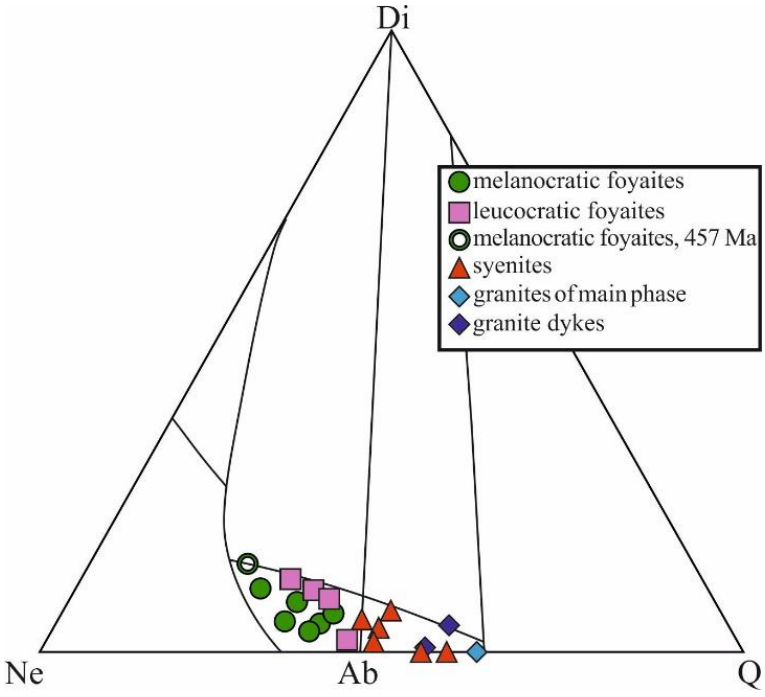

Figure 11. The normative Ne-Di-Q triangular diagram for the Saibar rocks [78]. The diagram illustrates that the syenites are intermediate between foyaites and granites. Ne = nepheline, Di = diopside, Ab = albite, Q = quartz.

Foyaite compositions are plotted in the Ne-Di-Ab field, while the compositions of all varieties of syenite, as well as granites, are located in the Di-Ab-Q field. At the same time, syenite compositions occupy an intermediate field between foyaites and granite compositions. Thus, gradual geological transitions from nepheline to quartz-bearing magmatic rocks cannot be explained by any regularity in crystallization differentiation of either the initial foyaite or initial syenite magma due to the existence of an insurmountable chemical barrier between nepheline-normative and quartz-normative melts. Moreover, among all rocks there are no correlations between Mg# (Figure 8) and incompatible elements, which could be confidently explained by fractionation of mineral phases. The spidergrams among the compositions of all varieties of syenites also show compositions close to those of both melanocratic and leucocratic foyaites (Figure 9e,f). This similarity of compositions is especially clearly manifested in relation to Rb, Ba, Th, U, K, Nb, Ta, P, Zr, Hf, and Ti. At the same time, there are some features of REE differentiation for foyaites and for syenites. Foyaites differ from each other in LREE and MREE contents, while syenites differ from each other in LREE, MREE, and HREE contents. These data on the bulk composition of rocks contradict the formation model of syenites from the parent foyaite magma with relatively low SiO_2 concentrations. In this study, we considered additional mechanisms of formation of silica in under- and oversaturated magmas. Such a mechanism should be the contribution of the xenogenic component to the magmatic system corresponding to the composition of syenites, which would disrupt the course of differentiation. The assimilation by syenite magma of the limestone fragments of Cambrian host blocks confidently explains the appearance of nepheline magmas and rocks. Thus, the contribution of the calcium component to the parent syenite magma could cause a relative decrease in the SiO_2 content up to the unsaturation of the magmatic system. For example, if 3% CaO (7% $CaCO_3$) is added to the melt corresponding to the syenite (SBR 3/1), then its composition will shift towards the appearance of normative nepheline. During the differentiation of such magma, and primarily due to early crystallization and removal of anorthite plagioclase from the melt, a series of rocks richer in alkalis and, accordingly, nepheline can be formed. This is confirmed by the following reaction: $CaCO_3$ (calcite) + $Na(Al,Si)Si_3O_8$ (albite) +$1/2Al_2O_3$ (melt) = $CaAl_2Si_2O_8$ (anorthite) + $NaAlSiO_4$ (nepheline) + CO_2. The contribution of carbonate component will practically not change the trace element contents of the magmas (Table 2, hybrid melt); therefore, geochemically, foyaites remain similar to syenites. Generally, they are also more enriched in Sr, which is a typical trace element of carbonate rocks. The discovery of foyaite outcrops in different sites of the Saibar intrusion, regardless of their distance from the contact zone with the host limestones, indicates a random distribution of the supposed limestone fragments in the magma chamber.

In contrast to the foyaitic sites, granites of the main phase are confined to the endocontact zone, which directly indicates the interaction of syenite magma with host rocks. Accordingly, both syenite and foyaite samples are characterized by a general enrichment in REEs, which correlates with the appearance of its leucocratic types. On the contrary, granites of the endocontact have depleted geochemical characteristics in comparison with other rocks of the Saibar intrusion (Figure 9a,b). Their element concentration is close to the average composition of the continental crust, as well as to the composition of the host intrusive felsic rocks, and occupies the position of a hybrid melt formed during the interaction of syenite magma with such host rocks.

Evaluating the regularities of magmatic evolution in this time interval, we must note an increase in the total alkalinity of felsic rocks. This is evidenced by the composition of the latest granite dykes. The composition of dyke granites is close to syenites in terms of the contents of Rb, Ba, K, Nb, Ta, Sr, and P, but they are enriched in REE concentrations (Figure 9c,d). This indicates the fractionation of mafic alkaline minerals of syenite magma without significant interaction with host crustal rocks. The weak Zr-Hf and Ti negative anomaly in the dyke granites indicates the early crystallization of titanium-bearing minerals.

Thus, geochemical data indicate a disruption of the differentiation process during the evolution of syenite magma and a change in its composition during the assimilation of different host crustal rocks. Our conceptual scenario assumes sites with captured blocks of carbonate rocks were formed in different segments of the intrusion remote from the endocontact zone. Differentiation of the syenite magma and an increase in its total alkalinity and desilication occurred, leading to the formation of foyaites, including distinguished melanocratic and leucocratic types, differing in the pattern of distribution of incompatible elements.

The combination of fractionation and assimilation is indicated by the isotopic composition of oxygen, in particular the $\delta^{18}O$ enrichment of alkali feldspars of syenites and granites of the endocontact zone.

Generally, the εNd(t) vs. age (Ma) diagram for the examined rocks shows that the Nd isotopic compositions are plotted in the field of Nd isotopic evolutions for Early Paleozoic granites of Central Asia, including the Early Paleozoic intrusions of the Kuznetsk Alatau (Figure 11; [48,75–77]). This assumes potential contaminants for Ordovician syenite magmas. At the same time, high εNd(t) values coincide with the isotopic neodymium characteristics for the Early Paleozoic mafic rocks and syenites related to the withinplate setting of the eastern Altai-Sayan region [79]. All these data point to the participation of magmas of a crustal and mantle nature during the formation of the Saibar intrusion.

5.2. Geodynamic Setting

Ordovician syenites are involved in the geological structure of volcano-plutonic areas, which are distributed in the mountainous frame of the Minusinsk Trough and more widely throughout the eastern part of the Altai-Sayan fold belt. As shown previously [33,80,81], these areas are composed of magmatic rocks with a wide range of SiO_2 content. Their geochemical and isotopic (Sr, Nd) characteristics reflect the interaction of mantle and crustal sources, which occurs both on active continental margins and in areas of withinplate magmatism with the participation of a mantle plume [82]. At the same time, geological data indicate a passive-margin geodynamic setting [83] and the withinplate position of magmatic areas. This geological restriction allows us to conclude that Ordovician magmatism was most likely determined by the effect of a mantle plume on the continental lithosphere in the northern part of the Altai-Sayan fold belt. This conclusion is consistent with the geochemical features of rocks of the Saibar intrusion, which are moderate and alkaline in nature; enrichment in most lithophile elements; and a clear geochemical difference from the composition of the crust and their affinity to the A-type granitoids.

6. Conclusions

The obtained geological and isotope-geochemical data for the Saibar intrusion rocks showed the following:

1. The Saibar intrusion is composed of dominant syenites, as well as few bodies of melanocratic and leucocratic nepheline syenites (foyaites) and endocontact granites. These rocks form the main magmatic phases. In addition, there are dykes of granites and mafic rocks. The U-Pb age of zircons in the melanocratic foyaites is estimated at 457 Ma.

2. The geological characteristics of mafic rocks indicate their corresponding formation in relation to the rocks of the main intrusion phase, which restricts the possibility of reconstructing of the parent magma composition. Accordingly, it is possible to discuss only that part of the magmatic evolution of parent magmas, which corresponds to syenites, foyaites, and all varieties of felsic rocks. The main phases of the Saibar intrusion were formed by a combination of fractionation and interaction of syenite magmas with host rocks. The foyaites appeared due to the fractionation and removal of Ca-rich plagioclase from the melt during the assimilation of host carbonate rocks. The composition of granite (main phase) was determined by the interaction with host intrusive felsic rocks in the endocontact zone. Dyke granite was formed by differentiation of syenite magma without a marked contribution of the host continental crust.

3. The geological affinity (age of formation, presence of nepheline rocks) of the Saibar intrusion with the Ordovician intrusions of the alkaline Altai-Sayan province makes it possible to associate its rocks with the evolution of mafic magmas, which occurred at levels of the magmatic system inaccessible to observation. The origin of such magmas was associated with the effect of a mantle plume on the continental lithosphere of the Altai-Sayan fold belt.

Author Contributions: Conceptualization, A.A.V., A.E.I. and V.V.Y.; Data curation, A.A.V.; Funding acquisition, A.A.V. and A.E.I.; Investigation, A.A.V., A.E.I., T.Y.K., A.V.N. and O.Y.P.; Methodology, S.I.D. and N.G.R.; Project administration, A.A.V.; Visualization, T.Y.K., O.Y.P., S.I.D. and E.P.D.; Writing—original draft, A.A.V.; Writing—review & editing, A.A.V., A.E.I. and V.V.Y. All authors have read and agreed to the published version of the manuscript.

Funding: Isotope-geochemical research reported was funded by RFBR (project numbers 19-05-00300 and 19-17-00019). Geochronological studies and clarification of the geological structure of the Saibar intrusion were carried out at the expense of the State Task of the Ministry of Science of the Russian Federation (project numbers 0284-2021-0006, 0330-2016-0003, and FMMN-2021-0006).

Data Availability Statement: Data available in a publicly accessible repository that does not issue DOIs.

Acknowledgments: The authors wish to acknowledge the valuable contribution of analytical groups from Irkutsk, St. Petersburg, and Ulan-Ude to element and isotope determinations. We would like to thank Olga Kryukova (krukova25@mail.ru) for thorough revision of the text in English. The authors are deeply grateful to the reviewers for allowing us to improve this paper.

Conflicts of Interest: The authors declare no conflict of interest.

References

1. Rocks, I. *Classification, Nomenclature, Petrography*; Bogatikov, O.A., Gon'shakova, V.I., Eds.; Nauka: Moscow, Russia, 1983; Volume 1, pp. 1–372. (In Russian)
2. Condie, K.C. *Mantle Plumes and Their Record in Earth History*; Cambridge University Press: Cambridge, UK, 2001; pp. 1–305.
3. Ernst, R.E. *Large Igneous Provinces*; Cambridge University Press: Cambridge, UK, 2014; pp. 1–667.
4. Burke, K.; Dewey, J. Plume-generated triple junctions: Key indicators in applying plate tectonics to old rocks. *J. Geol.* **1973**, *81*, 406–433. [CrossRef]
5. Pirajno, F. Intracontinental anorogenic alkaline magmatism and carbonatites, associated mineral systems and the mantle plume connection. *Gondwana Res.* **2015**, *27*, 1181–1216. [CrossRef]
6. Yashina, R.M. *Alkaline Magmatism in Orogenic Areas (Case of the Southern Periphery of the Siberian Craton)*; Nauka: Moscow, Russia, 1982; pp. 1–274. (In Russian)
7. Sheimann, Y.M.; Apeltsin, F.R.; Nechaeva, E.A. *Alkaline Intrusions, Their Placement and Associated Mineralization*; Gosgeoltekhizdat: Moscow, Russia, 1961; pp. 1–176. (In Russian)
8. Sheimann, Y.M. *Essays on Deep Geology*; Nedra: Moscow, Russia, 1968; pp. 1–232. (In Russian)
9. Litvinovsky, B.A.; Zanvilevich, A.N.; Burdukov, I.V.; Karmanov, N.S. Syenites as a product of fractional crystallization of alkaline-basaltic magma of the Oshurkovsky intrusion, Transbaikalia. *Russ. Petrol.* **1998**, *6*, 30–52.
10. Allen, C.M.; Chappell, B.W. Assosiation of I type granites with rift related alkali magmatism in central coastal Queensland, Australia. *Geol. Soc. Am. Abstr. Programs* **1992**, *24*, 43.
11. Lubala, R.T.; Frick, C.; Roders, J.H.; Walraven, F. Petrogenesis of syenites and granites of Schiel Alkaline complex, Northern Transvaal, South Africa. *J. Geol.* **1994**, *102*, 307–309. [CrossRef]
12. Huang, W.L.; Wyllie, P.J. Phase relationships of S-type granite with H_2O to 35 kbar: Muscovite granite from Harney Peak, South Dakota. *J. Geoph. Res.* **1981**, *86*, 10515–10529. [CrossRef]
13. Brown, P.E.; Becker, S.M. Fractionation, hybridisation and magma-mixing in the Kialineq centre, East Greenland. *Contrib. Mineral. Petrol.* **1986**, *92*, 57–70. [CrossRef]
14. Sheppard, S. Hybridization of shoshonitic lamprophyre and calc-alkaline granite magma in the early Proterozoic Mt Bundey igneous suite, Northern Territory. *Aust. J. Earth Sci.* **1995**, *42*, 173–185. [CrossRef]
15. Barker, F.; Wones, D.R.; Sharp, W.N.; Desborough, G.A. The Pikes Peak batholith, Colorado front range, and a model for the origin of the gabbro-anorthosite-syenite-potassic granite suite. *Precambrian Res.* **1975**, *2*, 97–160. [CrossRef]
16. Dorias, M. Compositional variations in pyroxens and amphiboles of the Belkmap Moutain complex, New Hampshire: Evidens for origin of silica-saturated alkaline rocks. *Am. Mineral.* **1990**, *75*, 1092–1105.
17. Kröner, A.; Kovach, V.; Belousova, E.; Hegner, E.; Armstrong, R.; Dolgopolova, A.; Sun, M. Reassessment of continental growth during the accretionary history of the Central Asian Orogenic Belt. *Gondwana Res.* **2014**, *25*, 103–125. [CrossRef]

18. Sengör, A.C.; Natal'in, B.A.; Burtman, V.S. Evolution of the Altaid tectonic collage and Palaeozoic crustal growth in Eurasia. *Nature* **1993**, *364*, 299–306. [CrossRef]
19. Windley, B.F.; Alexeiev, D.V.; Xiao, W.; Kröner, A.; Badarch, G. Tectonic models for accretion of the Central Asian Orogenic Belt. *J. Geol. Soc. Lond.* **2007**, *164*, 31–47. [CrossRef]
20. Coleman, R.G. Continental growth of North West China. *Tectonics* **1989**, *8*, 621–635. [CrossRef]
21. Kröner, A.; Hegner, E.; Lehmann, B.; Heinhorst, J.; Wingate, M.T.D.; Liu, D.Y.; Ermelov, P. Palaeozoic arc magmatism in the Central Asian Orogenic Belt of Kazakhstan: SHRIMP zircon ages and whole-rock Nd isotopic systematics. *Asian Earth Sci.* **2008**, *32*, 118–130. [CrossRef]
22. Rytsk, E.Y.; Kovach, V.P.; Yarmolyuk, V.V.; Kovalenko, V.I. Structure and evolution of the continental crust in the Baikal Fold Region. *Geotectonic* **2007**, *41*, 440–464. [CrossRef]
23. Windley, B.F.; Kröner, A.; Guo, J.; Qu, G.; Li, Y.; Zhang, C. Neoproterozoic to Paleozoic geology of the Altai orogen, NW China: New zircon age data and tectonic evolution. *J. Geol.* **2002**, *110*, 719–739. [CrossRef]
24. Yarmolyuk, V.V.; Kovalenko, V.I.; Kovach, V.P.; Rytsk, E.Y.; Kozakov, I.K.; Kotov, A.B.; Sal'nikova, E.B. Early Stages of the Paleoasian Ocean formation: Results of geochronological, isotopic, and geochemical investigations of Late Riphean and Vendian-Cambrian complexes in the Central Asian fold belt. *Dokl. Earth Sci.* **2006**, *411*, 1184–1189. [CrossRef]
25. Yarmolyuk, V.V.; Kovalenko, V.I.; Kozlovskii, A.M.; Kovach, V.P.; Sal'nikova, E.B.; Kovalenko, D.V.; Kotov, A.B.; Kudryashova, E.A.; Lebedev, V.I.; Eenzhin, G. Crust-forming processes in the Hercynides of the Central Asian foldbelt. *Petrology* **2008**, *16*, 679–709. [CrossRef]
26. Yarmolyuk, V.V.; Kovach, V.P.; Kovalenko, V.I.; Salnikova, E.B.; Kozlovskii, A.M.; Kotov, A.B.; Yakovleva, S.Z.; Fedoseenko, A.M. Composition, sources, and mechanism of continental crust growth in the Lake Zone of the Central Asian Caledonides: I. Geological and geochronological data. *Petrology* **2011**, *19*, 55–78. [CrossRef]
27. Yarmolyuk, V.V.; Kuz'min, M.I.; Vorontsov, A.A. Convergent boundaries of the West Pacific type and their role in the formation of the Central Asian fold belt. *Russ. Geol. Geophys.* **2013**, *54*, 1427–1441. [CrossRef]
28. Yarmolyuk, V.V.; Kuz'min, M.I.; Ernst, R.E. Intraplate geodynamics and magmatism in the evolution of the Central Asian Orogenic Belt. *J. Asian Earth Sci.* **2014**, *93*, 158–179. [CrossRef]
29. Wang, Z.W.; Pei, F.P.; Xu, W.L.; Cao, H.H.; Wang, Z.J.; Zhang, J. Tectonic evolution of the eastern Central Asian Orogenic Belt: Evidence from zircon U–Pb–Hf isotopes and geochemistry of early Paleozoic rocks in Yanbian region, NE China. *Gondwana Res.* **2016**, *38*, 334–350. [CrossRef]
30. Liu, Y.; Li, W.; Feng, Z.; Wen, Q.; Neubauer, F.; Liang, C. A review of the Paleozoic tectonics in the eastern part of Central Asian Orogenic Belt. *Gondwana Res.* **2017**, *43*, 123–148. [CrossRef]
31. Zhao, G.; Wang, Y.; Huang, B.; Dong, Y.; Li, S.; Zhang, G.; Yu, S. Geological reconstructions of the East Asian blocks: From the breaking of Rodinia to the assembly of Pangea. *Earth Sci. Rev.* **2018**, *186*, 262–286. [CrossRef]
32. Vrublevskii, V.V.; Grinev, O.M.; Izokh, A.E.; Travin, A.V. Geochemistry, isotope triad (Nd–Sr–O), and ^{40}Ar–^{39}Ar age of Paleozoic alkaline mafic intrusions of the Kuznetsk Alatau (by the example of the Belaya Gora pluton). *Russ. Geol. Geophys.* **2016**, *57*, 592–602. [CrossRef]
33. Vrublevskii, V.V. Sources and geodynamic setting of petrogenesis of the Middle Cambrian Upper Petropavlovka alkaline basic pluton (Kuznetsk Alatau, Siberia). *Russ. Geol. Geophys.* **2015**, *56*, 379–401. [CrossRef]
34. Vrublevskii, V.V.; Gertner, I.F.; Tishin, P.A.; Bayanova, T.B. Age range of zircon and sources of alkaline rocks Kurgusul intrusive, Kuznetsk Alatau: First U–Pb (Shrimp 2) Isotope and Sm–Nd Data. *Dokl. Earth Sci.* **2014**, *459*, 601–606. (In Russian) [CrossRef]
35. Vrublevskii, V.V.; Krupchatnikov, V.I.; Izokh, A.E.; Gertner, I.F. Alkaline Rocks and Carbonatites of Gorny Altai (Edelweiss complex): Indicator of Early Paleozoic Pluma Magmatism in the Central Asian Folding Belt. *Russ. Geol. Geophys.* **2012**, *53*, 945–963. [CrossRef]
36. Vrublevskii, V.V.; Izokh, A.E.; Polyakov, G.V.; Gertner, I.F.; Yudin, D.S.; Krupchatnikov, V.I. Early Paleozoic alkaline magmatism of Gorny Altai: ^{40}Ar-^{39}Ar-Geochronological evidence of the Edelweiss complex. *Dokl. Earth Sci.* **2009**, *427*, 96–100. [CrossRef]
37. Makarenko, N.A.; Kotel'nikov, A.D. The Kashpar Cambrian-Ordovik gabbro-diorite-quartzmontsodiorite-syenite Complex-New Petrography Department on the Eastern Slope of the Kuznetsk Alatau. *Geosph. Stud.* **2018**, *2*, 52–71. (In Russian)
38. Vrublevskii, V.V.; Gertner, I.F.; Gutiérrez-Alonso, G.; Hofmann, M.; Grinev, O.M.; Tishin, P.A. Isotope (U-Pb, Sm–Nd, Rb–Sr) geochronology of alkaline basic plutons of the Kuznetsk Alatau. *Russ. Geol. Geophys.* **2014**, *55*, 1264–1277. [CrossRef]
39. Vrublevskii, V.V.; Kotel'nikov, A.D.; Rudnev, S.N.; Krupchatnikov, V.I. Evolution of the Paleozoic granitoid magmatism in the Kuznetsk Alatau: New geochemical and U-Pb (SHRIMP-II) isotope data. *Russ. Geol. Geophys.* **2016**, *57*, 225–246. [CrossRef]
40. Vrublevskii, V.V.; Gertner, I.F.; Gutiérrez-Alonso, G.; Hofmann, M.; Grinev, O.M.; Mustafaev, A. Multiple intrusion stages and mantle sources of the Paleozoic Kuznetsk Alatau alkaline province, Southern Siberia: Geochemistry and Permian U–Pb, Sm–Nd ages in the Goryachegorsk ijolite-foyaite intrusion. *Int. Geol. Rev.* **2020**, 1–17. [CrossRef]
41. Mustafayev, A.A.; Gertner, I.F.; Serov, P.A. Features of geology and composition of rocks from the alkaline-gabbroic University intrusion (NE Kuznetsk Alatau ridge, Siberia). *Earth Environ. Sci.* **2017**, *319*, 012026.
42. Mustafayev, A.A.; Gertner, I.F.; Ernst, R.E.; Serov, P.A.; Kolmakov, Y.V. The Paleozoic-Aged University Foidolite-Gabbro Pluton of the Northeastern Part of the Kuznetsk Alatau Ridge, Siberia: Geochemical Characterization, Geochronology, Petrography and Geophysical Indication of Potential High-Grade Nepheline Ore. *Minerals* **2020**, *10*, 1128. [CrossRef]

43. Mustafaev, A.; Gertner, I. Isotope-geochemical (Sm–Nd, Rb–Sr, REE, HFSE) composition of the University foidolite-gabbro pluton, Kuznetsk Alatau ridge, Siberia. *Vestn. St. Petersburg Univer. Earth Sci.* **2020**, *65*, 1–33. (In Russian)
44. Kononova, V.A. *Jakupirangite-Urtite Series of Alkaline Rocks*; Nauka: Moscow, Russia, 1976; pp. 1–215. (In Russian)
45. Andreeva, E.D.; Kononova, V.A.; Sveshnikova, E.V.; Yashina, R.M. Alkaline rocks. In *Igneous Rocks*; Bogatikov, O.A., Kononova, V.A., Borsuk, A.M., Gon'shakova, V.I., Kovalenko, V.I., Laz'ko, E.E., Sharkov, E.V., Eds.; Nauka: Moscow, Russia, 1984; Volume 2, pp. 1–415. (In Russian)
46. Ernst, R.E.; Rodygin, S.A.; Grinev, O.M. Age correlation of Large Igneous Provinces with Devonian biotic crises. *Glob. Planet. Chang.* **2020**, *185*, 103097. [CrossRef]
47. Perfilova, O.Y.; Makhlaev, M.L.; Sidoras, S.D. Ordovician volcanic-plutonic association in structures of the folded surrounding of the Minusa depression. *Russ. Lithosphere* **2004**, *3*, 137–152. (In Russian)
48. Rudnev, S.N. *Early Paleozoic Granitoid Magmatism of the Altai-Sayan Folded Region and the Lake Zone of Western Mongolia*; SB RAS: Novosibirsk, Russia, 2013; pp. 1–300. (In Russian)
49. Kosorukov, A.P. Devonian alkaline-syenite complex of the Sydo-Erbinsk depression and its mountain frame. In *Magmatic Complexes of Folded Regions of Southern Siberia*; Polyakov, G.V., Ed.; Nauka: Novosibirsk, Russia, 1981; Volume 509, pp. 128–157. (In Russian)
50. Vologdin, A.G. Geological research in 1924 in the area of the town of Saybar and Bolshe-Telek Baytak. Russia. *News Geol. Comm.* **1925**, *44*, 18–43. (In Russian)
51. Luchitsky, I.V. *Volcanism and Tectonics of the Devonian Depressions of the Minusinsk Intermountain Trough*; Academy of Sciences of the USSR: Moscow, Russia, 1960; pp. 1–276. (In Russian)
52. Saranchina, G.M. Alkaline rocks of the Saybar intrusion (Western Siberia, Krasnoyarsk Region). *Uchenye Zap. LSU* **1940**, *45*, 253–287. (In Russian)
53. Fedoseev, G.S.; Polyakov, G.V. Intrusions of granites and syenites of the eastern framing of the Sydo-Erbinsk and South-Minusinsk depressions. In *Middle Paleozoic Intrusions of Granites and Syenites of the Kuznetsk Alatau and the North-Western Part of the Eastern Sayan*; Kuznetsov, Y.A., Ed.; Nauka: Novosibirsk, Russia, 1974; Volume 177, pp. 148–207. (In Russian)
54. Fedorov, E.E. To the question of syenite intrusion of the Tubino-Sisimsky region (Krasnoyarsk Territory). *Mater. VSEGEI (Common Ser.)* **1948**, *8*, 106–112. (In Russian)
55. Edelstein, Y.S. Geological outline of the Minusinsk depression and adjacent parts of the Kuznetsk Alatau and East Sayan. In *Essays on the Geology of Siberia*; Obruchev, V.A., Ed.; Publishing House of the USSR Academy of Sciences: Leningrad, Russia, 1932; pp. 1–59. (In Russian)
56. Kostyuk, V.P.; Guletskaya, E.S. To mineralogy of the Saybar intrusion (Eastern Sayan). *Russ. Geol. Geophys.* **1967**, *7*, 43–50. (In Russian)
57. Krogh, T.E. A low-contamination method for hydrothermal dissolution of zircon and extraction of U and Pb for isotopic age determinations. *Geochim. Cosmochim. Acta* **1973**, *37*, 485–494. [CrossRef]
58. Ludwig, K.R. PBDAT—A Computer Program for Processing Pb-U-Th Isotope Data, Version 1.22. In *Open-File Report*; United States Geological Survey: Reston, CF, USA, 1991; Volume 38, pp. 88–542.
59. Ludwig, K.R. User's Manual for Isoplot/Ex, Version 2.10. In *A Geochronological Toolkit for Microsoft Excel*; Berkley Geochronology Center Special Publication: Berkeley, CA, USA, 1999; Volume 1, pp. 1–46.
60. Steiger, R.H.; Jäger, E. Subcommission on geochronology: Convention on the use of decay constants in geo- and cosmochronology. *Earth Planet. Sci. Lett.* **1977**, *36*, 359–362. [CrossRef]
61. Stacey, J.S.; Kramers, J.D. Approximation of Terrestrial Lead Isotope Evolution by a 2-Stage Model. *Earth Plan. Sci. Lett.* **1975**, *26*, 207–221. [CrossRef]
62. Afonin, V.P.; Gunicheva, T.N.; Piskunova, L.F. *X-Ray Fluorescence Silicate Analysis*; Nauka: Novosibirsk, Russia, 1984; pp. 1–228. (In Russian)
63. Sharp, Z.D. A laser-based microanalytical method for the in situ determination of oxygen isotope ratios of silicates and oxides. *Geochim. Cosmochim. Acta* **1990**, *54*, 1353–1357. [CrossRef]
64. Richard, P.; Shimizu, N.; Allègre, C.J. $^{143}Nd/^{146}Nd$ a natural tracer: An Application to Oceanic Basalts. *Earth Plan. Sci. Lett.* **1976**, *31*, 269–278. [CrossRef]
65. Pin, C.; Briot, D.; Bassin, C.; Poitrasson, F. Concominant separation of strontium and samarium–neodymium for isotopic analysis in silicate samples, based on specific extraction chromatography. *Anal. Chim. Acta* **1994**, *298*, 209–217. [CrossRef]
66. Makishima, A.; Nagender, B.; Nakamura, E. New sequential separation procedure for Sr, Nd and Pb isotope ratio measurement in geological material using MC-ICP-MS and TIMS. *Geochem. J.* **2008**, *42*, 237–246. [CrossRef]
67. Yang, Y.-H.; Chu, Z.Y.; Wu, F.-Y.; Xia, L.-W.; Yang, J.-H. Precise and accurate determination of Sm, Nd concentrations and Nd isotopic compositions in geological samples by MC-ICP-MS. *J. Anal. At. Spectrom.* **2010**, *26*, 1237–1244. [CrossRef]
68. Tanaka, T.; Togashi, S.; Kamioka, H.; Amakawa, H.; Kagami, H.; Hamamoto, T.; Kunimaru, T. JNdi-1: A neodymium isotopic reference in consistency with LaJolla neodymium. *Chem. Geol.* **2000**, *168*, 279–281. [CrossRef]
69. Sharpenok, L.N.; Kostin, A.E.; Kukharenko, E.A. TAS-diagram the sum of alkalis-silica for chemical classification and diagnostics of plutonic rocks. *Reg. Geol. Metallog.* **2013**, *56*, 40–50. (In Russian)
70. Maniar, P.D.; Piccoli, P.M. Tectonic discrimination of granitoids. *Geol. Soc. Am. Bull.* **1989**, *101*, 635–643. [CrossRef]
71. Frost, B.R.; Frost, C.D. A geochemical classifcation for feldspathic igneous rocks. *J. Petrol.* **2008**, *49*, 1955–1969. [CrossRef]

72. Sun, S.; McDonough, W.F. Chemical and isotopic systematics of oceanic basalts: Implications for mantle composition and processes Basins. In *Magmatism in the Ocean Basins*; Special Publications 42; Saunders, A.D., Norry, M.J., Eds.; Geological Society of London: London, UK, 1989; pp. 313–345.
73. King, P.L.; White, A.J.R.; Chappell, B.W.; Allen, C.M. Characterization and Origin of Aluminous A-type Granites from the Lachlan Fold Belt, Southeastern Australia. *J. Petrol.* **1997**, *38*, 371–391. [CrossRef]
74. Rudnick, R.L.; Gao, S. Composition of the Continental Crust. In *Treatise on Geochemistry*; Holland, H.D., Turekian, K.K., Rudnick, R.L., Eds.; Elsevier Ltd.: Oxford, UK, 2003; Volume 3, pp. 1–56.
75. Kovalenko, V.I.; Yarmolyuk, V.V.; Kovach, V.P. Sources of Phanerozoic granitoids of Central Asia: Sm-Nd isotope data. *Geochem. Int.* **1996**, *8*, 628–640.
76. Kovalenko, V.I.; Yarmolyuk, V.V.; Kozakov, I.K.; Kovach, V.P.; Kotov, A.B.; Salnikova, E.B. Sm-Nd isotopic provinces of the Earth's crust in Central Asia. *Dokl. Earth Sci.* **1996**, *348*, 220–222. (In Russian)
77. Kovalenko, V.I.; Yarmolyuk, V.V.; Kovach, V.P.; Kotov, A.B.; Kozakov, I.K.; Salnikova, E.B.; Larin, A.M. Isotope provinces, mechanisms of generation and sources of the continental crust in the Central Asian mobile belt: Geological and isotopic evidence. *Asian Earth Sci.* **2004**, *23*, 605–627. [CrossRef]
78. Schairer, J.F.; Yoder, H.S., Jr. The nature of residual liquids from crystallization, with data on the system nepheline-diopside-silica. *Am. J. Sci.* **1960**, *258*, 273–283.
79. Lykhin, D.A.; Yarmolyuk, V.V.; Vorontsov, A.A. Age, composition and sources of rocks and ores of the Okunevsky fluorite-leukophane deposit (Western Sayan): To assess the contribution of magmatism to the formation of ore mineralization. *Geol. Ore Depos.* **2019**, *61*, 37–61. (In Russian) [CrossRef]
80. Vorontsov, A.A.; Perfilova, O.Y.; Kruk, N.N. Geodynamic setting, structure, and composition of continuous trachybasalt-trachiandesite-rhyolite series in the northe of Altai-Sayan area: The role of crust-mantle interaction in continental magma formation. *Russ. Geol. Geophys.* **2018**, *59*, 1640–1659. [CrossRef]
81. Vorontsov, A.A.; Perfilova, O.Y.; Kruk, N.N.; Tarasyuk, A.S. Late Ordovician volcanism of the northern part of Altai-Sayan area and its geodynamic nature. *Dokl. Earth Sci.* **2019**, *485*, 347–354. [CrossRef]
82. Yarmolyuk, V.V.; Kovalenko, V.I. Deep geodynamics and mantle plumes: Their role in the formation of the Central Asian fold belt. *Russ. Petrol.* **2003**, *11*, 504–531.
83. Berzin, N.A.; Kungurtsev, L.V. Geodynamic interpretation of geological complexes of the Altai-Sayan region. *Russ. Geol. Geophys.* **1996**, *37*, 63–81.